



Stress singularities and transverse stresses near edges of doubly curved laminated shells using TSNDT and stress recovery scheme



P.H. Shah, R.C. Batra*

Department of Biomedical Engineering and Mechanics, M/C 0219, Virginia Polytechnic Institute and State University, Blacksburg, VA 24061, USA

ARTICLE INFO

Article history:

Received 28 April 2016

Received in revised form

5 November 2016

Accepted 16 November 2016

Available online 19 November 2016

Keywords:

TSNDT

Doubly curved laminated shells

Transverse stresses

Stress singularity

ABSTRACT

A third order shear and normal deformable plate/shell theory (TSNDT) and a stress recovery scheme (SRS) are used to predict stress singularities near edges of doubly curved composite laminated shells deformed statically with tangential and normal tractions applied on the shell major surfaces. In fluid-structure interaction problems both tangential and normal tractions may simultaneously act on the fluid-structure interface. The accurate computation of all six stress components is important for ascertaining a structure's load carrying capacity. In the TSNDT the three displacement components at a point are expressed as complete polynomials of degree three in the thickness coordinate. The boundary-value problems are numerically solved by using an in-house developed finite element code. Results for six problems involving different boundary conditions at the edges and different surface tractions on the two major surfaces are presented. For each problem studied, the computed stresses at interior points located at a distance greater than 0.1% of the span from an edge are found to at most differ by 5% from those obtained by either analytical or numerical (with a commercial software) solutions of the 3-D linear elasticity theory equations. The order of the stress singularity near an edge and boundary layers close to bounding surfaces are well captured; the region of stress singularity extends from the edge only till 0.4% of the edge length. Advantages of using the TSNDT include considering general tractions on bounding surfaces and finding a reasonably accurate solution, including singular stresses near the edges, with considerably fewer degrees of freedom than those needed to analyze the corresponding 3-D problem.

© 2016 Elsevier Masson SAS. All rights reserved.

1. Introduction

Theories developed to analyze infinitesimal deformations of doubly curved linear elastic shells of uniform thickness can broadly be categorized as classical, shear deformation and shear and normal deformation. Classical theories such as Love's first approximation theory (LFAT) (Love, 1888), Donnell's (1933), Sanders' (1959) and Flugge's (1973) shell theories neglect the transverse shear and the transverse normal strains and give very good results for thin shallow shells. The shear deformation theories account for the transverse shear deformations and predict well responses of moderately thick shells. The shear and normal deformation theories consider both transverse shear and normal deformations, account for changes in thickness, and usually do not require a correction factor. A challenge in plate theories especially for laminated structures is the accurate determination of the

transverse shear and the transverse normal stresses, stress singularities near the edges where failure may initiate and propagate inwards, boundary layer effects in moderately thick structures, and stresses at points on interfaces between adjoining layers.

A shell is called shallow (deep) if its rise equals at most (at least) one-fifth of its smallest planform dimension (Qatu, 2004). It is usually regarded as thick, moderately thick, and thin if the ratio of the thickness to the smallest planform length and/or the smaller radius of curvature is at least 1/10, between 1/10 and 1/20, and at most 1/20, respectively (Qatu, 2004).

The first order shear deformation theory (FSDT) assumes constant transverse shear strains across the shell thickness and generally requires a shear correction factor for studying deformations of moderately thick shells. Higher order shear deformation theories (HSDTs) (Lo et al., 1977; Murty, 1977; Reddy and Liu, 1985; Liew and Lim, 1996; Xiao-ping, 1996) may provide accurate solutions for deformations of thick shells without requiring a shear correction factor. Nearly all HSDTs are descendants of either Mindlin's or Reissner's theories. For example, Mindlin (1951)

* Corresponding author.

E-mail addresses: spriyal@vt.edu (P.H. Shah), rbatra@vt.edu (R.C. Batra).

expanded the three displacements in terms of Taylor series about their values at the mid-surface and retained terms of order K in the thickness coordinate, z . Instead of polynomials in z , other authors have used trigonometric functions of z to express through-the-thickness variations of the in-plane displacements. Naghdi (1973) and Antman (1972) have reviewed historical developments of plate and shell theories, and proposed their own theories.

Reddy and Liu (1985), Liew and Lim (1996) and Xiao-ping (1996) proposed a third order shear deformation theory (TSDT) in which the transverse displacement is constant across the shell thickness and the in-plane displacements are complete polynomials of degree three in z . This leads to a parabolic distribution of transverse shear strains along the thickness and zero transverse normal strain. By requiring the transverse shear stresses to vanish on the two major surfaces, they reduced the number of unknowns in the theory. The need to consider both transverse shear and transverse normal deformations has been pointed out by Reissner (1947) and Koiter (1960). Reissner stated in 1947 that for sandwich shells with $(tE_f)/(hE_c) \gg 1$ both transverse shear and transverse normal deformations should be considered. Here t and E_f (h and E_c) equal, respectively, the thickness and the longitudinal modulus of the face sheet (core). Based on energy considerations Koiter (1960) recommended that any refinement of the LFAT must simultaneously consider both transverse shear and transverse normal stresses. For a thermally loaded thick plate (length/thickness = 5) made of an inhomogeneous linear elastic material with material moduli only varying in the thickness direction, Vel and Batra (2002) found that the deviation in the transverse deflection from the exact solution equals 26%, 26% and 28% for the classical plate theory, the FSDT and the TSDT, respectively. These large errors are possibly due to neglecting the transverse normal strain in the three theories. For the problem studied by Vel and Batra (2002), Qian and Batra (2004) found that a 5th order shear and normal deformable plate theory gave results very close to the analytical solution of the problem. For 100 K temperature difference between the top and the bottom surfaces of the plate, the transverse displacement of the centroid of the top surface of the plate equalled twice of that of the centroid of the bottom surface signifying an average transverse normal strain of $\sim 10^{-3}$. These examples signify the need for considering transverse normal deformations in a plate/shell theory.

Following Mindlin and Medick (1959), Vidoli and Batra (2000) and Batra and Vidoli (2002), amongst others, expressed all three displacements as complete polynomials of degree K (K is a variable) in z , and studied deformations of piezoelectric and orthotropic linear elastic plates for values of K up to 7. They deduced the constitutive relation for the plate by using either the Hellinger–Prange–Reissner principle or from the 3-D constitutive relations and the plate theory displacements; the corresponding theories are called “mixed” and “compatible”, respectively. The mixed theory exactly satisfies surface traction boundary conditions (BCs) on the two major surfaces. Batra and Aimmanee (2005) used the K^{th} order mixed theory to analyze free vibrations of thick plates. Using a compatible theory Qian et al. (2003) found that $K = 3$ provides excellent values up to the 4th bending frequency of a moderately thick plate with a rather coarse distribution of nodes. The compatible plate theory with $K = 3$ has been termed as the third order shear and normal deformable theory (TSNDT). Qian and Batra (2004) have generalized the compatible theory to plates composed of thermoelastic materials. Bert and Broutman (1980), Leissa (1973), Qatu (2004), Qatu et al. (2012) and Liew et al. (1997), amongst others, have reviewed shell theories. Whereas Qian et al. (2003) and Batra et al. (2002) have analyzed the effect of K on frequencies, stresses, deflections and wave propagation in thick plates, Carrera et al. (2014) have proposed a unified formulation in which the three displacement components are expressed in terms of a generic

function, $F(z)$, in the thickness coordinate, z , as follows:

$$u_i(x, y, z) = F_{ij}(z) u_j(x, y) \quad (i = 1, 2, 3, j = 1, 2, \dots, N)$$

Here summation on the repeated index j is implied over the range of values of j . In the TSNDT, $N = 4$ and the function $F_{ij}(z) = z^{j-1}$ for $i = 1, 2, 3$ and $j = 1, 2, 3, 4$. Carrera et al. (2014) have proposed varying N , the expressions for $F_{ij}(z)$ and $u_j(x, y)$ to compute a solution within a pre-specified tolerance. This approach uses the least number of variables for a given plate, lamination scheme, domain discretization and BCs but is computationally more expensive than other approaches mentioned above.

Vel and Batra (1999) have used the Eshelby–Stroh formalism to analytically solve the 3-D linear elasticity theory (LET) equations for laminated plates with possibly different BCs on each ply edges, and have compared their results with predictions from different plate theories. The boundary conditions at the edges were satisfied in the sense of Fourier series. The analytical solution exhibited singularities in stresses at points on the free edges that can induce delamination between the adjoining layers. These stress singularities had earlier been predicted by Bogy (1968) and Dundurs (1969), and the order of singularity depends upon the elastic moduli of the two adjoining layers.

Deformations of a laminated shell (or plate) can be analyzed either by using an equivalent single layer (ESL) theory in which the shell is envisaged to be made of a homogeneous material or by using a layer-wise (LW) theory. In an ESL (LW) theory, the number of unknowns equals (the number of layers times) that for a monolithic shell. The transverse normal and the transverse shear stresses computed using constitutive relations in an ESL theory may not satisfy the continuity of surface tractions across interfaces between adjoining layers. However, in a LW theory these continuity conditions are built into the weak formulation of the problem. Carrera (2003), Ambartsumian (1962, 2002), Reddy (1993), Reddy and Arciniega (2004) and Kapania (1989), amongst others, have reviewed various ESL and LW theories for laminated plates and shells.

A commonly used approach is to find in-plane stresses from constitutive relations and the plate/shell theory displacements and compute transverse stresses by using either a one-step or a two-step stress recovery scheme (SRS). In the one-step SRS, transverse stresses are found by integrating the three equilibrium equations starting from a major surface and satisfying the traction continuity conditions at each interface between two adjoining layers. Pagano (1970) computed inter-laminar stresses in a laminated plate by using the one-step SRS in conjunction with the classical laminated plate theory (CLPT) and found them to agree well with the corresponding 3-D LET solutions. Pryor and Barker (1971) used the FSDT and Lo et al. (1978) employed a TSDT with the cubic and the quadratic variations of the in-plane and the transverse displacements, respectively, to analyze deformations of laminates and computed transverse shear stresses by using the one-step SRS. Using the SRS and TSNDT, Shah and Batra (2015) computed transverse stresses in laminates subjected to different traction BCs on their major surfaces. Tornabene et al. (2015) used a higher order shell theory to analyze deformations of doubly curved laminated shells and employed the generalized differential quadrature method to solve the 3-D LET equations at points along the shell thickness for computing transverse stresses. Rather than using the 3-D equilibrium equations, Chaudhuri and Seide (1987) employed 1-D quadratic shape functions through the thickness of each layer of the laminate to compute transverse shear stresses.

In the two-step SRS, transverse stresses are iteratively computed. For example, Noor et al. (1990, 1991) used a predictor-corrector approach to find inter-laminar stresses. In the predictor

phase the in-plane stresses are obtained by using constitutive relations and the plate theory displacements with a shear correction factor, transverse stresses are obtained with the one-step SRS, and the corresponding strain energies are computed. In the corrector phase from predicted values of either transverse shear stresses or strain energies of transverse shear deformations, either through-the-thickness distributions of displacements or the shear correction factor are refined until convergence within a prescribed tolerance is achieved.

Wang and Li (1992) employed the method of separation of variables and the 3-D LET to study deformations of laminated cylindrical shells subjected to thermal and mechanical loads. They deduced equilibrium equations for unknown displacements for each layer and computed inter-laminar stresses by making displacements and stresses satisfy BCs and the interface continuity conditions. Wu and Kuo (1992) proposed a local third order lamination theory in which the local displacement components are represented as high order polynomials in the thickness coordinate within each ply. They introduced displacement continuity constraints at the interface between the adjoining layers into the potential energy functional through Lagrange multipliers thereby increasing the number of unknowns. Rohwer et al. (2005) and Kant and Swaminathan (2000), amongst others, have reviewed different techniques to compute inter-laminar transverse stresses in laminates.

A reasonably accurate estimate of interlaminar stresses and edge singularities is needed to delineate damage and failure initiation and propagation from the edges. Once delamination ensues new traction free surfaces are created and stresses at the edges of the delaminated zone may exhibit singularities. Xiao and Batra (2014) and Batra and Xiao (2013) have used a LW TSNDT to analyze the initiation and propagation of mode-I and mode-II delamination in laminated and sandwich curved beams subjected to water slamming loads.

Here we study static infinitesimal deformations of laminated composite doubly curved shells using the compatible ESL theory

$$\begin{aligned} \epsilon_{11} &= \frac{1}{H_1} \left(\frac{\partial u_1}{\partial y_1} + \frac{u_3}{R_1} \right), & \epsilon_{22} &= \frac{1}{H_2} \left(\frac{\partial u_2}{\partial y_2} + \frac{u_3}{R_2} \right), & 2\epsilon_{12} &= \frac{1}{H_1} \frac{\partial u_2}{\partial y_1} + \frac{1}{H_2} \frac{\partial u_1}{\partial y_2}, \\ 2\epsilon_{13} &= \frac{1}{H_1} \left(\frac{\partial u_3}{\partial y_1} - \frac{u_1}{R_1} \right) + \frac{\partial u_1}{\partial y_3}, & 2\epsilon_{23} &= \frac{1}{H_2} \left(\frac{\partial u_3}{\partial y_2} - \frac{u_2}{R_2} \right) + \frac{\partial u_2}{\partial y_3}, & \epsilon_{33} &= \frac{\partial u_3}{\partial y_3} \end{aligned} \quad (2)$$

with no shear correction factor and the TSNDT displacement field. We compute in-plane stresses from constitutive relations and the shell theory displacements, and the transverse normal and the transverse shear stresses by the one-step SRS. Using in-house developed code based on the finite element (FE) formulation of the problem, we study several problems for laminated shells specified with different BCs including combination of clamped, simply supported and traction free edges and subjected to different loads that include (i) uniform and sinusoidal normal tractions on a major surface, (ii) equal and opposite uniform tangential tractions on the top and the bottom surfaces, and (iii) combined uniform normal and tangential tractions on a major surface. The focus is on ascertaining transverse stresses, boundary layer effects and stress singularities, if any, at interface points near the edges. It is found that for each problem studied, all stress components agree well with those from either analytical or numerical solutions of the 3-D LET equations. Furthermore, stress singularities, if present, near the edges and boundary layers near bounding surfaces are well captured.

2. Problem formulation

A laminated doubly curved shell, shown in Fig. 1, is composed of N perfectly bonded layers with each layer made of a homogeneous, orthotropic and linear elastic material. The total thickness and the two constant principal radii of curvature of the mid-surface of the shell are denoted by h , R_{1m} and R_{2m} , respectively. Let (y_1, y_2, y_3) be orthogonal curvilinear coordinates such that $y_1 = \text{constant}$ and $y_2 = \text{constant}$ are curves of principal curvature on the mid-surface, $y_3 = 0$. The arc lengths of the shell at the mid-surface in the y_1 - and the y_2 - directions are a and b , respectively, and the corresponding planform lengths are l_1 and l_2 , respectively. We use fixed rectangular Cartesian coordinate axes (X_1, X_2, X_3) and (x_1, x_2, x_3) with the X_3 - and the x_3 - axes parallel to the y_3 - axis, to denote position vectors of a point by \mathbf{X} and \mathbf{x} in the reference and the current configurations, respectively.

The components G_{ij} of the metric tensor in the reference configuration are given by

$$G_{ij} = \mathbf{A}_i \cdot \mathbf{A}_j, \quad \mathbf{A}_i = \frac{\partial \mathbf{X}}{\partial y_i} \quad (i = 1, 2, 3) \quad (1)$$

where $\mathbf{A}_i \cdot \mathbf{A}_j$ equals the inner product between vectors \mathbf{A}_i and \mathbf{A}_j . We note that for the orthogonal curvilinear coordinate system, G_{ij} is non-zero only when $i = j$. Let $(\bar{\mathbf{e}}_1, \bar{\mathbf{e}}_2, \bar{\mathbf{e}}_3)$ be unit base vectors associated with the curvilinear coordinate axes (y_1, y_2, y_3) . That is, $\bar{\mathbf{e}}_i = \frac{\mathbf{A}_i}{H_i}$ (no sum on i), where $H_1 = \left(1 + \frac{y_3^2}{R_1^2}\right)$, $H_2 = \left(1 + \frac{y_3^2}{R_2^2}\right)$, $H_3 = 1$, R_1 and R_2 are radii of curvature at (y_1, y_2, y_3) of the planes $y_2 = \text{constant}$ and $y_1 = \text{constant}$, respectively.

The displacement \mathbf{u} of a point is given by $\mathbf{u} = \mathbf{x} - \mathbf{X}$. The physical components of the infinitesimal strain tensor in the curvilinear coordinate system are given by (Saada, 2009)

where ϵ_{ii} ($i = 1, 2, 3$; no sum on i) is the normal strain along the y_i -direction, ϵ_{12} is the in-plane shear strain, and ϵ_{13} and ϵ_{23} are the transverse shear strains.

In the TSNDT the displacement, u_i , at a point is expressed as a complete polynomial of degree 3 in the thickness coordinate, y_3 . That is,

$$\mathbf{d}(y_1, y_2, y_3) = (y_3)^i \mathbf{d}_i(y_1, y_2) \quad (i = 0, 1, 2, 3) \quad (3)$$

Unless mentioned otherwise, a repeated index implies summation over the range of the index. In Eqn. (3) $\mathbf{d} = [u_1 \ u_2 \ u_3]^T$. The 12-dimensional vector $\bar{\mathbf{d}} = [\mathbf{d}_0, \mathbf{d}_1, \mathbf{d}_2, \mathbf{d}_3]$ is called the vector of generalized displacements at a point on shell's mid-surface.

We substitute for u_i from Eqn. (3) into Eqn. (2) to obtain

$$\epsilon = \mathbf{Z}_i(y_3) \mathbf{L}_i \mathbf{d}_i(y_1, y_2) \quad (i = 0, 1, 2, 3) \quad (4)$$

where

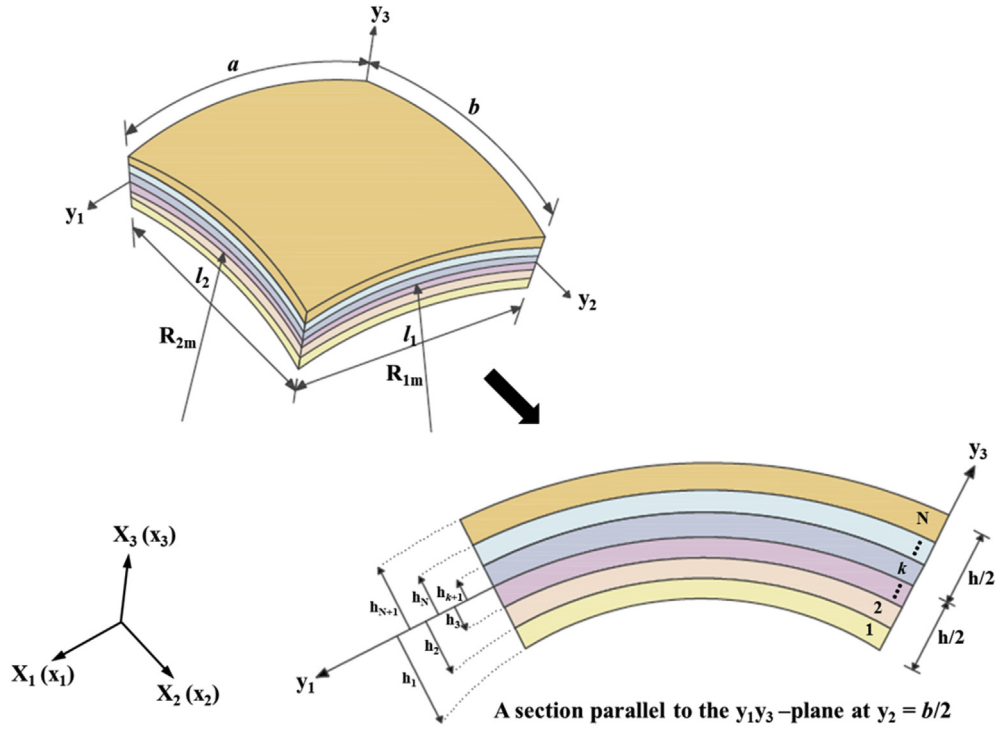


Fig. 1. Geometry and coordinate system of a doubly curved laminated shell. Colored figures are only on the web version of the paper.

$$\epsilon = [\epsilon_{11} \ \epsilon_{22} \ \epsilon_{33} \ 2\epsilon_{23} \ 2\epsilon_{13} \ 2\epsilon_{12}]^T \quad (4.1)$$

and the operator matrix L and matrices Z_i ($i = 0, 1, 2, 3$) are defined as

$$L^T = \begin{bmatrix} \frac{\partial}{\partial y_1} & 0 & \frac{\partial}{\partial y_2} & 0 & 0 & 0 & 1 & 0 & 0 \\ 0 & \frac{\partial}{\partial y_2} & 0 & \frac{\partial}{\partial y_1} & 0 & 1 & 0 & 0 & 0 \\ 0 & 0 & 0 & 0 & 1 & 0 & 0 & \frac{\partial}{\partial y_2} & \frac{\partial}{\partial y_1} \end{bmatrix} \quad (4.2)$$

$$Z_i = \begin{bmatrix} \frac{(y_3)^i}{H_1} & 0 & 0 & 0 & \frac{(y_3)^i}{R_1 H_1} & 0 & 0 & 0 & 0 \\ 0 & \frac{(y_3)^i}{H_2} & 0 & 0 & \frac{(y_3)^i}{R_2 H_2} & 0 & 0 & 0 & 0 \\ 0 & 0 & 0 & 0 & i (y_3)^{i-1} & 0 & 0 & 0 & 0 \\ 0 & 0 & 0 & 0 & 0 & \frac{i (y_3)^{i-1} + (i-1) (y_3)^i / R_2}{H_2} & 0 & \frac{(y_3)^i}{H_2} & 0 \\ 0 & 0 & 0 & 0 & 0 & 0 & \frac{i (y_3)^{i-1} + (i-1) (y_3)^i / R_1}{H_1} & 0 & \frac{(y_3)^i}{H_1} \\ 0 & 0 & \frac{(y_3)^i}{H_2} & \frac{(y_3)^i}{H_1} & 0 & 0 & 0 & 0 & 0 \end{bmatrix} \quad (4.3)$$

Similar to components of the strain tensor, we write components of the Cauchy stress tensor as a 6-D vector

$$\sigma = [\sigma_{11} \ \sigma_{22} \ \sigma_{33} \ \sigma_{23} \ \sigma_{13} \ \sigma_{12}]^T \quad (5)$$

The constitutive relation (Hooke's law) for a linear elastic material is

$$\sigma_{ij} = C_{ijmn} \epsilon_{mn}, \quad C_{ijmn} = C_{mnij} = C_{jimn}, \quad (i, j, m, n = 1, 2, 3) \quad (6)$$

where \mathbf{C} is the fourth-order elasticity tensor having 21 independent components for a general anisotropic material. For an orthotropic, a transversely isotropic and an isotropic material, the independent components of \mathbf{C} reduce, respectively, to 9, 5 and 2.

With respect to the material principal axes Eqn. (6) for an orthotropic material of layer k becomes

$$\begin{Bmatrix} \sigma_{11}^k \\ \sigma_{22}^k \\ \sigma_{33}^k \\ \sigma_{23}^k \\ \sigma_{13}^k \\ \sigma_{12}^k \end{Bmatrix} = \begin{bmatrix} C_{1111}^k & C_{1122}^k & C_{1133}^k & 0 & 0 & 0 \\ C_{1122}^k & C_{2222}^k & C_{2233}^k & 0 & 0 & 0 \\ C_{1133}^k & C_{2233}^k & C_{3333}^k & 0 & 0 & 0 \\ 0 & 0 & 0 & C_{2323}^k & 0 & 0 \\ 0 & 0 & 0 & 0 & C_{1313}^k & 0 \\ 0 & 0 & 0 & 0 & 0 & C_{1212}^k \end{bmatrix} \times \begin{Bmatrix} \epsilon_{11}^k \\ \epsilon_{22}^k \\ \epsilon_{33}^k \\ 2\epsilon_{23}^k \\ 2\epsilon_{13}^k \\ 2\epsilon_{12}^k \end{Bmatrix} \quad (7)$$

where quantities for the k^{th} layer are indicated by the superscript k . In the global coordinate axes (y_1, y_2, y_3) C_{ijmn} are computed by using the tensor transformation rules for the stress and the strain tensors, and the 6×6 matrix may be fully populated. For the TSNDT, the elastic constants in Eqn. (7) are the same as those used in the LET, i.e., they are not modified to satisfy $\sigma_{33} = 0$ as is often done in the classical shell theories.

We use the principle of minimum potential energy, given by Eqn. (8), to derive equations governing static deformations of the shell:

$$\delta \Pi = 0 \quad (8)$$

where δ is the variational operator and Π is the potential energy of the shell which in the absence of body forces is given by

$$\Pi = \frac{1}{2} \sum_{k=1}^N \int_{\Omega^k} (\epsilon^k)^T \sigma^k d\Omega^k - \int_{\bar{A}} \mathbf{d}^T \bar{\mathbf{f}} d\bar{A} \quad (8.1)$$

in which Ω^k represents the region occupied by the k^{th} layer, and \bar{A} is the part of the bounding surfaces of the shell on which surface traction, $\bar{\mathbf{f}}$, is specified. Points on the remainder of the boundary of the domain, $\Omega = \sum_{k=1}^N \Omega^k$, occupied by the shell have either null tractions (i.e., are on a free surface) or have displacements prescribed on them. The work done by reaction forces at points of the boundary where displacements are prescribed is not included in Eqn. (8) because variations in the prescribed displacements there are null.

We substitute in Eqn. (8.1) for \mathbf{d} in terms of \mathbf{d}_i ($i = 0, 1, 2, 3$) from Eqn. (3), for σ^k in terms of ϵ^k from Eqn. (7), and for ϵ^k in terms of the generalized displacements defined on the shell mid-surface from Eqn. (4). In the resulting expression for $\delta \Pi$, we integrate with respect to y_3 over the shell thickness to obtain the following:

$$\delta \Pi = \int_0^b \int_0^a \delta \mathbf{d}_i^T \mathbf{L}^T \mathbf{D}_{ij} \mathbf{L} \mathbf{d}_j dy_1 dy_2 - \int_{\bar{A}} \delta \mathbf{d}_i^T (y_3)^i \bar{\mathbf{f}} d\bar{A} = 0 \quad (i, j = 0, 1, 2, 3) \quad (9)$$

where

$$\mathbf{D}_{ij} = \sum_{k=1}^N \int_{h_k}^{h_{k+1}} \mathbf{z}_i^T \mathbf{C}^k \mathbf{z}_j dy_3 \quad (9.1)$$

We discretize the mid-surface, $\mathfrak{R} = [0, a] \times [0, b]$, of the shell into an FE mesh of N_e disjoint 8-node iso-parametric elements where the region \mathfrak{R}_e occupied by the element e is given by, $\mathfrak{R}_e = [y_1^e, y_1^{e+1}] \times [y_2^e, y_2^{e+1}]$. Thus $\delta \Pi$ equals the sum of integrals over each element. The 12-dimensional vector $\bar{\mathbf{d}}$ of generalized displacements at a point in an element is expressed in terms of values of $\bar{\mathbf{d}}$ at the 8-nodes using the FE basis functions. Thus the total number of unknowns in the problem equals $12N_{\text{node}}$ where N_{node} equals the number of nodes. We note that in the FE formulation of the corresponding 3-D problem, the number of unknowns equals $3N_{\text{node}}^*$, where N_{node}^* equals the number of nodes in the 3-D problem. Since $N_{\text{node}}^* \gg N_{\text{node}}$, the total number of unknowns for the TSNDT will be much less than that for the 3-D problem.

We write the vector of generalized variables \mathbf{d}_j ($j = 0, 1, 2, 3$) of a point in an element e in terms of the 24-D vector $\mathbf{d}_j^e = [\mathbf{d}_1^e, \mathbf{d}_2^e, \dots, \mathbf{d}_8^e]$ containing values of \mathbf{d}_j at the 8-nodes of the element as follows:

$$\mathbf{d}_j = \Phi \mathbf{d}_j^e \quad (j = 0, 1, 2, 3) \quad (10)$$

Here

$$\Phi = [\psi_1 \mathbf{I} \quad \psi_2 \mathbf{I} \quad \dots \quad \psi_8 \mathbf{I}], \quad (10.1)$$

is a (3×24) matrix containing shape functions $(\psi_1, \psi_2, \dots, \psi_8)$ associated with the 8 nodes of the element and \mathbf{I} is a (3×3) identity matrix. Following the terminology in Chapter 5 of Bathe's book (Bathe, 1996), we employ 8-node iso-parametric elements for which shape functions for the 8-node master element are given in Fig. 5.4 of Bathe's book.

Substituting for \mathbf{d}_m ($m = 0, 1, 2, 3$) from Eqn. (10) into Eqn. (9), the first variation of the total potential energy of a typical element is given by

$$\delta \Pi^e = \delta \mathbf{d}_i^e{}^T \mathbf{K}_{ij}^e \mathbf{d}_j^e - \delta \mathbf{d}_i^e{}^T (\mathbf{T}_i^{+e} + \mathbf{T}_i^{-e} + \mathbf{P}_i^{+e} + \mathbf{P}_i^{-e} + \mathbf{Q}_i^{+e} + \mathbf{Q}_i^{-e}) = 0 \quad (i, j = 0, 1, 2, 3) \quad (11)$$

The elemental stiffness matrices \mathbf{K}_{ij}^e and the elemental load vectors $\mathbf{T}_i^{\pm e}$, $\mathbf{P}_i^{\pm e}$, $\mathbf{Q}_i^{\pm e}$ ($i, j = 0, 1, 2, 3$) appearing in Eqn. (11) are given by

$$\mathbf{K}_{ij}^e = \int_{y_2^e}^{y_2^{e+1}} \int_{y_1^e}^{y_1^{e+1}} \mathbf{B}^T \mathbf{D}_{ij} \mathbf{B} dy_1 dy_2,$$

where

$$\mathbf{B} = \mathbf{L}\Phi \tag{11.1}$$

$$\begin{aligned} \mathbf{T}_i^{\pm e} &= \int_{y_2^e}^{y_2^{e+1}} \int_{y_1^e}^{y_1^{e+1}} (y_3)^i \Phi^T \mathbf{f}^{\pm} dy_1 dy_2, \\ \mathbf{P}_i^{\pm e} &= \int_{y_2^e}^{y_2^{e+1}} \int_{-h/2}^{h/2} (y_3)^i \Phi^T \mathbf{p}^{\pm} dy_3 dy_2, \\ \mathbf{Q}_i^{\pm e} &= \int_{y_1^e}^{y_1^{e+1}} \int_{-h/2}^{h/2} (y_3)^i \Phi^T \mathbf{q}^{\pm} dy_3 dy_1 \end{aligned} \tag{11.2}$$

where \mathbf{f}^+ and \mathbf{f}^- are surface tractions prescribed on the top and the bottom surfaces, respectively, of the shell; and \mathbf{p}^+ , \mathbf{p}^- , \mathbf{q}^+ and \mathbf{q}^- are surface tractions prescribed on the edge surfaces, $y_1 = a$, $y_1 = 0$, $y_2 = b$ and $y_2 = 0$, respectively. $\mathbf{P}_i^{\pm e}$ and $\mathbf{Q}_i^{\pm e}$ are evaluated only for those elements that share a boundary with the shell edges.

Recalling that variations in generalized displacements are arbitrary except at nodes where displacements are prescribed, Eqn. (11) yields the following equilibrium equations for an FE:

$$\begin{aligned} \mathbf{K}_{00}^e \mathbf{d}_0^e + \frac{1}{2}(\mathbf{K}_{01}^e + \mathbf{K}_{10}^{eT}) \mathbf{d}_1^e + \frac{1}{2}(\mathbf{K}_{02}^e + \mathbf{K}_{20}^{eT}) \mathbf{d}_2^e + \frac{1}{2}(\mathbf{K}_{03}^e + \mathbf{K}_{30}^{eT}) \mathbf{d}_3^e &= \mathbf{F}_0^e \\ \frac{1}{2}(\mathbf{K}_{10}^e + \mathbf{K}_{01}^{eT}) \mathbf{d}_0^e + \mathbf{K}_{11}^e \mathbf{d}_1^e + \frac{1}{2}(\mathbf{K}_{12}^e + \mathbf{K}_{21}^{eT}) \mathbf{d}_2^e + \frac{1}{2}(\mathbf{K}_{13}^e + \mathbf{K}_{31}^{eT}) \mathbf{d}_3^e &= \mathbf{F}_1^e \\ \frac{1}{2}(\mathbf{K}_{20}^e + \mathbf{K}_{02}^{eT}) \mathbf{d}_0^e + \frac{1}{2}(\mathbf{K}_{21}^e + \mathbf{K}_{12}^{eT}) \mathbf{d}_1^e + \mathbf{K}_{22}^e \mathbf{d}_2^e + \frac{1}{2}(\mathbf{K}_{23}^e + \mathbf{K}_{32}^{eT}) \mathbf{d}_3^e &= \mathbf{F}_2^e \\ \frac{1}{2}(\mathbf{K}_{30}^e + \mathbf{K}_{03}^{eT}) \mathbf{d}_0^e + \frac{1}{2}(\mathbf{K}_{31}^e + \mathbf{K}_{13}^{eT}) \mathbf{d}_1^e + \frac{1}{2}(\mathbf{K}_{32}^e + \mathbf{K}_{23}^{eT}) \mathbf{d}_2^e + \mathbf{K}_{33}^e \mathbf{d}_3^e &= \mathbf{F}_3^e \end{aligned} \tag{12}$$

where

$$\mathbf{F}_i^e = \mathbf{T}_i^{+e} + \mathbf{T}_i^{-e} + \mathbf{P}_i^{+e} + \mathbf{P}_i^{-e} + \mathbf{Q}_i^{+e} + \mathbf{Q}_i^{-e} \quad (i = 0, 1, 2, 3) \tag{12.1}$$

Eqns. (12) are assembled using the standard technique to obtain

$$\mathbf{K}\mathbf{U} = \mathbf{F} \tag{13}$$

In Eqn. (13) \mathbf{K} is the global stiffness matrix, \mathbf{U} the global vector of generalized nodal displacements, and \mathbf{F} the global load vector; their expressions are given by Eqn. (13.1). The vector \mathbf{F} of generalized nodal forces is work equivalent to surface tractions applied on the top, the bottom, and the edge surfaces of the shell. For an FE mesh of N_{node} nodes, before applying essential BCs, the length of vector \mathbf{U} equals $12 N_{\text{node}}$ since a node has 12 degrees of freedom.

Table 1
Nomenclature for boundary conditions specified at edges $y_1 = 0$ or a .

Notation	Name	BCs in the 3-D LET	BCs in the TSNDT
C	Clamped	$u_1 = 0, u_2 = 0, u_3 = 0$	$u_{1i} = 0, u_{2i} = 0, u_{3i} = 0$
S	Simply supported	$\sigma_{11} = 0, u_2 = 0, u_3 = 0$	$M_{11}^i = 0, u_{2i} = 0, u_{3i} = 0$
F	Traction free	$\sigma_{11} = 0, \sigma_{12} = 0, \sigma_{13} = 0$	$M_{11}^i = 0, M_{12}^i = 0, M_{13}^i = 0$

$$\begin{aligned} \mathbf{K} &= \begin{bmatrix} \mathbf{K}_{00} & \frac{1}{2}(\mathbf{K}_{01} + \mathbf{K}_{10}^T) & \frac{1}{2}(\mathbf{K}_{02} + \mathbf{K}_{20}^T) & \frac{1}{2}(\mathbf{K}_{03} + \mathbf{K}_{30}^T) \\ \frac{1}{2}(\mathbf{K}_{10} + \mathbf{K}_{01}^T) & \mathbf{K}_{11} & \frac{1}{2}(\mathbf{K}_{12} + \mathbf{K}_{21}^T) & \frac{1}{2}(\mathbf{K}_{13} + \mathbf{K}_{31}^T) \\ \frac{1}{2}(\mathbf{K}_{20} + \mathbf{K}_{02}^T) & \frac{1}{2}(\mathbf{K}_{21} + \mathbf{K}_{12}^T) & \mathbf{K}_{22} & \frac{1}{2}(\mathbf{K}_{23} + \mathbf{K}_{32}^T) \\ \frac{1}{2}(\mathbf{K}_{30} + \mathbf{K}_{03}^T) & \frac{1}{2}(\mathbf{K}_{31} + \mathbf{K}_{13}^T) & \frac{1}{2}(\mathbf{K}_{32} + \mathbf{K}_{23}^T) & \mathbf{K}_{33} \end{bmatrix} \\ \mathbf{U} &= \begin{bmatrix} \mathbf{U}_0 \\ \mathbf{U}_1 \\ \mathbf{U}_2 \\ \mathbf{U}_3 \end{bmatrix}, \quad \mathbf{F} = \begin{bmatrix} \mathbf{F}_0 \\ \mathbf{F}_1 \\ \mathbf{F}_2 \\ \mathbf{F}_3 \end{bmatrix} \end{aligned} \tag{13.1}$$

in which \mathbf{U}_0 , \mathbf{U}_1 , \mathbf{U}_2 and \mathbf{U}_3 are global vectors of generalized displacements.

We specify three types of BCs at a point on a shell edge. At edges $y_1 = 0$ and a , the definitions of these BCs in the 3-D LET and their equivalent in terms of variables of the TSNDT are given in Table 1.

In Table 1 and in Eqn. (14) below, the index i takes values 0, 1, 2 and 3, u_{1i} is the 1st component of vector \mathbf{d}_i appearing in Eq. (3), and

$$M_{1n}^i = \int_{-h/2}^{h/2} (y_3)^i \sigma_{1n} dy_3 \quad (n = 1, 2, 3) \tag{14}$$

Displacement (or essential) BCs applied at points on a shell edge are satisfied while solving the linear system of algebraic equations summarized in Eqn. (13).

3. Numerical solution of problems

We use the following values of elastic constants with respect to the material principal axes (Z_1, Z_2, Z_3). Values of elastic constants C_{ijmn} in Eqn. (6) are deduced from these by using the tensor transformation rules. The data set 1 and 2 are, respectively, for transversely isotropic and orthotropic materials. The Z_1 -axis is the axis of transverse isotropy for a transversely isotropic material.

Data set 1:

$$E_1 = 172.4 \text{ GPa}, \quad E_1/E_2 = 25, \quad E_3 = E_2, \quad G_{12} = G_{13} = 0.5E_2, \\ G_{23} = 0.2E_2, \quad \nu_{12} = \nu_{13} = \nu_{23} = 0.25$$

Data set 2:

$$E_1 = 251 \text{ GPa}, \quad E_2 = 48 \text{ GPa}, \quad E_3 = 7.5 \text{ GPa}, \\ G_{12} = 13.6 \text{ GPa}, \quad G_{13} = 12 \text{ GPa}, \quad G_{23} = 4.7 \text{ GPa}, \\ \nu_{12} = 0.036, \quad \nu_{13} = 0.25, \quad \nu_{23} = 0.171$$

Here E_1 denotes Young's modulus along the Z_1 -direction, and G_{12} (ν_{12}) the shear modulus (Poisson's ratio) in the Z_1Z_2 -plane.

When discussing below results we replace X_1, X_2 and X_3 by x, y

and z, respectively, and displacements u_1, u_2 and u_3 by u, v and w , respectively. To investigate the efficacy of the TSNDT, we compare for each problem studied results computed from the TSNDT with those obtained by analyzing 3-D deformations with either the commercial FE software, ABAQUS, or analytical solutions available in the literature. The following norms are used for quantifying errors in the TSNDT solutions.

$$\|e\|_0 = \left[\int_{s_1}^{s_2} [\alpha_{3-D}(s) - \alpha_{TSNDT}(s)]^2 ds \Big/ \int_{s_1}^{s_2} \alpha_{3-D}^2(s) ds \right]^{1/2} \quad (15)$$

$$\|e\|_{sup} = \sup_{s \in [s_1, s_2]} (|\alpha_{3-D}(s) - \alpha_{TSNDT}(s)| / |\alpha_{3-D}(s)|); \alpha_{3-D}(s) \neq 0 \quad (16)$$

Here subscripts TSNDT and 3-D denote, respectively, values of the variable found by using the TSNDT and the 3-D elasticity theory. We note that $\|e\|_{sup}$ is a stronger measure of the error than $\|e\|_0$ and these quantify, respectively, the maximum and the average relative differences between the two solutions over the interval $[s_1, s_2]$.

We compute the in-plane stresses ($\sigma_{xx}, \sigma_{yy}, \sigma_{xy}$) from constitutive relations and the TSNDT displacements and the transverse shear (σ_{xz}, σ_{yz}) and the transverse normal (σ_{zz}) stresses by using the one-step SRS; these are labeled “C” and “SRS”, respectively. As mentioned in the Introduction, in the SRS, the three equilibrium equations are integrated with respect to z starting from the bottom-most face with surface tractions prescribed there as “initial conditions”. At interfaces between two adjoining layers the traction continuity conditions are satisfied during integration of equilibrium equations. The difference between the computed and the applied surface tractions on the topmost surface can be regarded as a measure of the error in the numerical solution. While using the SRS, stress gradients are computed by first finding stresses at the 3×3 quadrature points in each FE on the shell surface $z = \text{constant}$, fitting a complete quadratic polynomial through their values at the 9-points by the least squares method, and then differentiating these polynomials with respect to x and y.

Unless mentioned otherwise, all layers of a laminate are of equal thickness, the displacement, w, and the stress, σ , are normalized as $\bar{w} = w(h^3/b^4)E_2/q_0$ and $\bar{\sigma} = \sigma/q_0$, respectively, where q_0 equals the maximum applied surface traction. The lamination scheme $\alpha_1/\alpha_2/\dots/\alpha_N$ with layer 1 being the bottom-most implies that fibers in the k^{th} layer are oriented at angle α_k measured counter-clockwise from the x- axis. Except when finding stress singularities at points near the edges that necessitates a much finer FE mesh, results from the TSNDT are computed using a uniform FE mesh of 25 elements in the x- and the y- directions (23,712 nodal degrees of freedom (DoF)) that provided a converged solution for most problems studied herein.

3.1. Comparison of the presently computed solution with that from the 3-D LET

We analyze deformations of a simply supported cross-ply laminated spherical ($R_{1m} = R_{2m} = R$) shell with normal tensile traction applied only on the top surface, and values of material parameters given by Data set 1.

3.1.1. Uniform surface traction, q_0

In Table 2 we have compared the non-dimensional deflection, \bar{w} , of the centroid of the mid-surface of the symmetric $0^\circ/90^\circ/90^\circ/0^\circ$ shell for $a = b, h = 40$ mm, $a/h = 100$ and 10, and different values of R/a obtained from the TSNDT, the 3-D LET solution of Fan and Zhang (1992) and the TSDT solution of Reddy and Liu (1985), and Fan and Zhang (1992). The entries in the column “Diff.” next to the TSNDT and the TSDT results are the difference between the values from the 3-D LET and the respective shell theory. For thin shells of $a/h = 100$, the three sets of results are in good agreement with each other. For $a/h = 10$ and $R/a = 1$, the TSDT and the TSNDT solutions differ from the 3-D LET solution by 12.6% and 6.6%, respectively. The maximum error in the TSNDT prediction for the other four problems is less than 2% whereas that for the TSDT is 11.7%. The results reported in Table 2 indicate that for moderately thick shells ($a/h = 10$), the centroidal displacements predicted by the TSDT are less than those by the TSNDT. Both for $a/h = 10$ and 100, the centroidal deflection of the shell increases with an increase

Table 2 Non-dimensional deflection, $\bar{w}(0.5a, 0.5b, 0) \times 10^3$, of the centroid of the mid-surface of the $0^\circ/90^\circ/90^\circ/0^\circ$ spherical shell with $a/b = 1, h = 40$ mm.

R/a	a/h = 100					a/h = 10				
	3-D LET (Fan and Zhang, 1992)	TSNDT	% Diff.	TSDT (Reddy and Liu, 1985; Fan and Zhang, 1992)	% Diff.	3-D LET (Fan and Zhang, 1992)	TSNDT	% Diff.	TSDT (Reddy and Liu, 1985; Fan and Zhang, 1992)	% Diff.
1	0.0722	0.0724	-0.28	0.0715	0.97	5.5323	5.8991	-6.63	4.8366	12.58
2	0.2857	0.2861	-0.14	0.2844	0.46	9.1212	9.2959	-1.92	8.0517	11.73
3	0.6265	0.6255	0.16	0.6246	0.30	10.3331	10.3163	0.16	9.1463	11.49
4	1.0585	1.0618	-0.31	1.0559	0.25	10.8207	10.706	1.06	9.5999	11.28
5	1.5392	1.5432	-0.26	1.5358	0.22	11.0535	10.8861	1.51	9.8249	11.12

Table 3 Non-dimensional deflection, $\bar{w}(0.5a, 0.5b, 0) \times 10^3$, at the centroid of the mid-surface of $0^\circ/90^\circ/0^\circ$ spherical shell; $R/a = 1, a/b = 1, h = 30$ mm.

a/h	3-D LET (Fan and Zhang, 1992)	TSNDT	% Diff.	TSDT (Reddy and Liu, 1985; Fan and Zhang, 1992)	% Diff.	FSDT (Fan and Zhang, 1992; Reddy, 1984) ($(k_1^2, k_2^2) = (0.7, 0.6)$)	% Diff.	FSDT (Fan and Zhang, 1992; Reddy, 1984) ($(k_1^2 = k_2^2 = 5/6)$)	% Diff.
100	0.0541	0.054241	-0.26	0.05351	1.09	0.05361	0.91	0.05361	0.91
100/3	0.4624	0.46871	-1.36	0.44185	4.44	0.44867	2.97	0.44801	3.11
20	1.1724	1.2055	-2.82	1.073	8.48	1.1144	4.95	1.1052	5.73
100/7	2.0863	2.167	-3.87	1.8231	12.62	1.9435	6.84	1.9024	8.81
100/9	3.1667	3.3048	-4.36	2.6473	16.40	2.8953	8.57	2.787	11.99
10	3.7676	3.9352	-4.45	3.0856	18.10	3.4152	9.35	3.2588	13.50
5	12.083	12.464	-3.15	8.6043	28.79	10.339	14.43	9.2536	23.42

Table 4

Non-dimensional deflection, $\bar{w}(0.5a, 0.5b, 0) \times 10^2$, at the centroid of the mid-surface of $[0^\circ/90^\circ/0^\circ/ \dots]$ spherical shell; $R/a = 2, a/b = 1, h = 10$ mm.

Number of layers, N		2	3	4	5	10
$a/h = 10$	3-D LET (Huang, 1994)	0.8533	0.6087	0.6128	0.5671	0.5495
	TSNDT	0.8645	0.6045	0.596	0.5529	0.5413
	%Diff.	-1.31	0.69	2.74	2.5	1.49
	HSDT* (Huang, 1994)	0.8567	0.6119	0.617	0.5696	0.5516
	%Diff.	-0.40	-0.53	-0.69	-0.44	-0.38
	HSDT** (Huang, 1994)	0.848	0.584	0.5673	0.5344	0.5221
	%Diff.	0.62	4.06	7.42	5.77	4.99
	TSDT (Reddy and Liu, 1985; Huang, 1994)	0.8207	0.5633	0.5471	0.5151	0.5031
	%Diff.	3.82	7.46	10.72	9.17	8.44
	3-D LET (Huang, 1994)	1.646	1.482	1.434	1.376	1.284
$a/h = 5$	TSNDT	1.65	1.445	1.31	1.249	1.183
	%Diff.	-0.24	2.5	8.65	9.23	7.87
	HSDT* (Huang, 1994)	1.683	1.519	1.498	1.404	1.315
	%Diff.	-2.25	-2.50	-4.46	-2.03	-2.41
	HSDT** (Huang, 1994)	1.615	1.42	1.228	1.217	1.148
	%Diff.	1.88	4.18	14.37	11.56	10.59
	TSDT (Reddy and Liu, 1985; Huang, 1994)	1.551	1.363	1.177	1.167	1.101
	%Diff.	5.77	8.03	17.92	15.19	14.25

in the shell curvature to edge length ratio, R/a , when $a = b$.

$$q(x, y) = q_0 \sin(\pi x/a) \sin(\pi y/b) \tag{17}$$

3.1.2. Sinusoidal surface tractions

For the top major surface subjected to the sinusoidal surface traction

we have listed in Table 3 the non-dimensional deflection at the centroid of the mid-surfaces of the symmetric $0^\circ/90^\circ/0^\circ$ shells with $R/a = 1, a = b, h = 30$ mm and different values of the a/h ratio

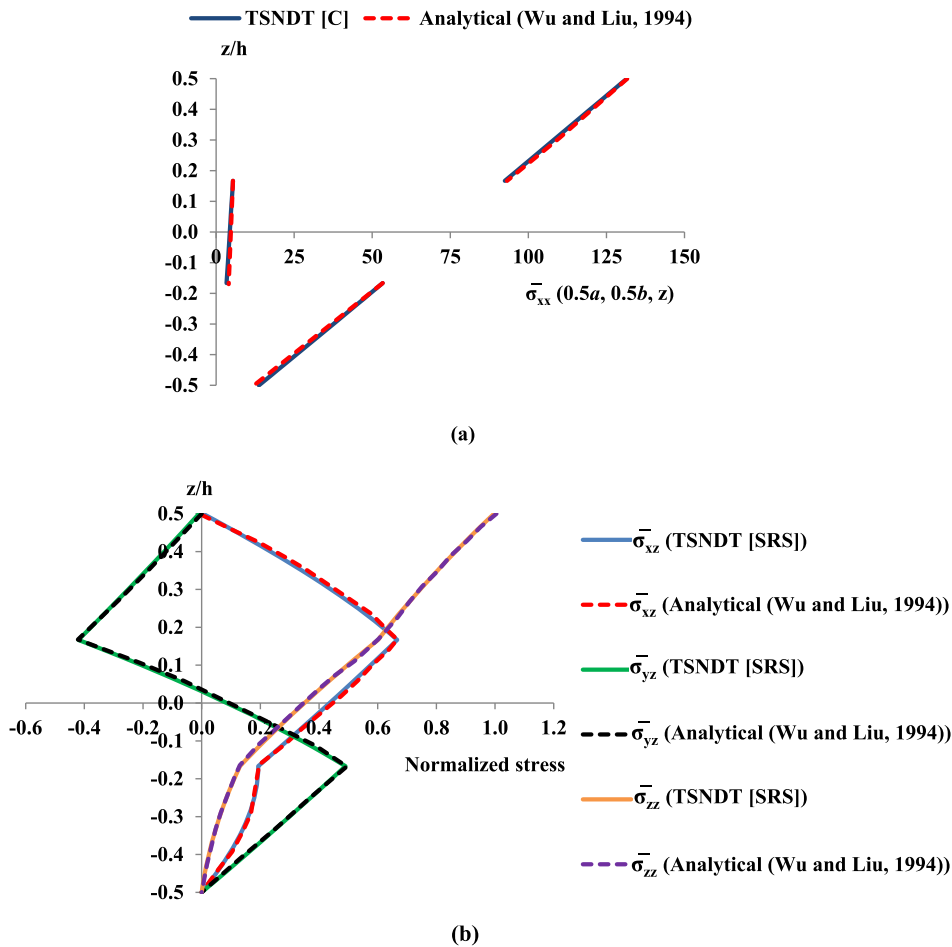


Fig. 2. For a simply supported $0^\circ/90^\circ/0^\circ$ spherical shell subjected to the sinusoidal tensile normal traction given by Eqn. (17) on the top surface, through-the-thickness distributions of (a) $\bar{\sigma}_{xx}(0.5a, 0.5b, z)$, (b) $\bar{\sigma}_{xz}(0, 0.5b, z)$, $\bar{\sigma}_{yz}(0.5a, 0, z)$, and $\bar{\sigma}_{zz}(0.5a, 0.5b, z)$. Stresses are normalized by q_0 . Analytical solutions are plotted using the data digitized from Wu and Liu (1994).

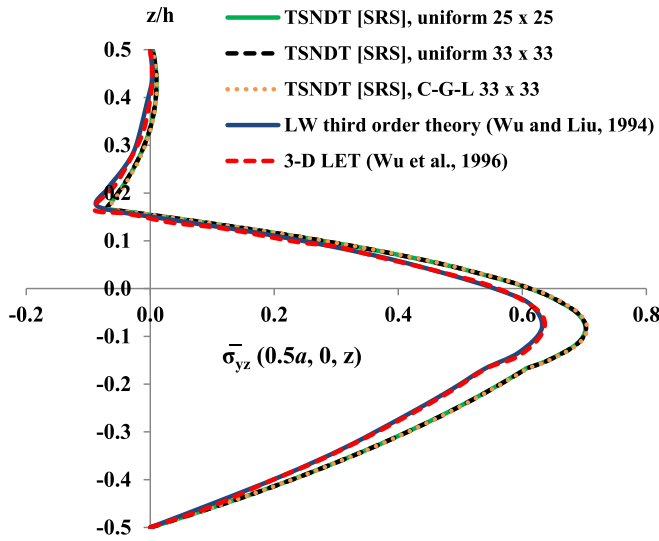


Fig. 3. For a simply supported $0^\circ/90^\circ/0^\circ$ spherical shell loaded on the top surface by sinusoidal normal tractions given by Eqn. (17), the through-the-thickness distribution of $\bar{\sigma}_{yz}(0.5a, 0, z)$. The stress is normalized by q_0 . Solutions from the LW third order theory and the 3-D LET are plotted using the data digitized from Wu and Liu (1994) and Wu et al. (1996), respectively.

obtained from the TSNDT, the TSDT (Reddy and Liu, 1985; Fan and Zhang, 1992), and the FSDT (Fan and Zhang, 1992; Reddy, 1984) with two sets of values for the shear correction factors (k_1, k_2) associated with (σ_{xz}, σ_{yz}) and compared these results with the corresponding 3-D LET solutions (Fan and Zhang, 1992). These results suggest that the error in the shell theory predictions increases with an increase in the ratio, a/h . The TSNDT predicted centroidal displacement has the least error (less than 4.5%) among the three shell theories considered. The maximum error in the centroidal displacements from the TSDT is 29% and from the FSDT is 23% and 10% for $k_1^2 = k_2^2 = 5/6$ and $(k_1^2, k_2^2) = (0.7, 0.6)$, respectively.

In Table 4 we have compared the non-dimensional deflection at the centroid of the mid-surface of $[0^\circ/90^\circ/0^\circ/ \dots]$ shells with $R/a = 2$, $h = 10$ mm, $a/h = 10$ and 5 and the number of layers $N = 2, 3, 4, 5$ and 10 obtained from the TSNDT, the 3-D LET (Huang, 1994), the HSDT of Huang (1994) and the TSDT of Reddy and Liu (1985) and of Huang (1994). We note that displacement fields for the HSDT and the TSDT are the same. However, unlike for the TSDT shear correction factors were used in the HSDT to obtain continuous transverse shear stresses at interfaces of the adjoining layers and no shallow shell approximations were made. The shear correction factors were iteratively varied to match the strain energy for the quasi 3-D transverse shear stresses and that of the shell theory transverse stresses within a prescribed tolerance. We note that values for “HSDT*” and “HSDT***” reported in Table 4 were obtained with and without using shear correction factors. The entry “Diff.” below a shell theory result denotes the difference between it and the 3-D LET result. The maximum difference between results from the TSNDT and the 3-D LET is 9.23% (2.74%) for $a/h = 5$ (10). For $a/h = 5$ (10), the corresponding differences in the centroidal deflections found from the HSDT without using shear correction factors and the TSDT are 14.37% (7.42%) and 17.92% (10.72%), respectively. However, when shear correction factors are used with the HSDT this difference reduces to 4.46% (0.69%) for $a/h = 5$ (10). Results listed in Table 4 indicate that the TSNDT generally gives lower errors in centroidal deflections than those from the TSDT and the HSDT**

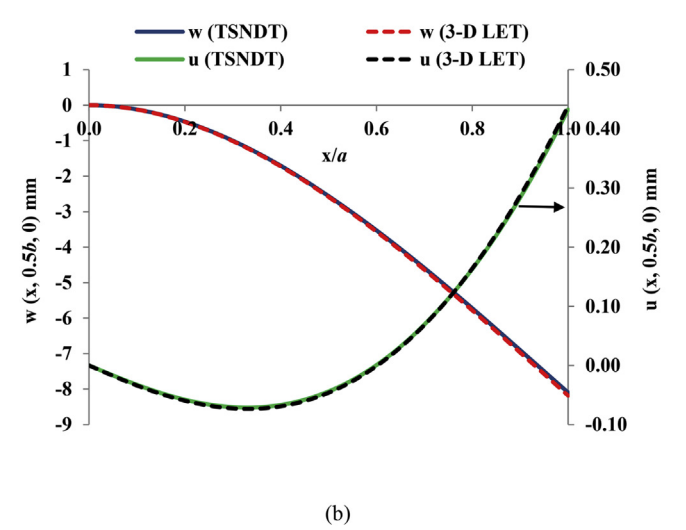
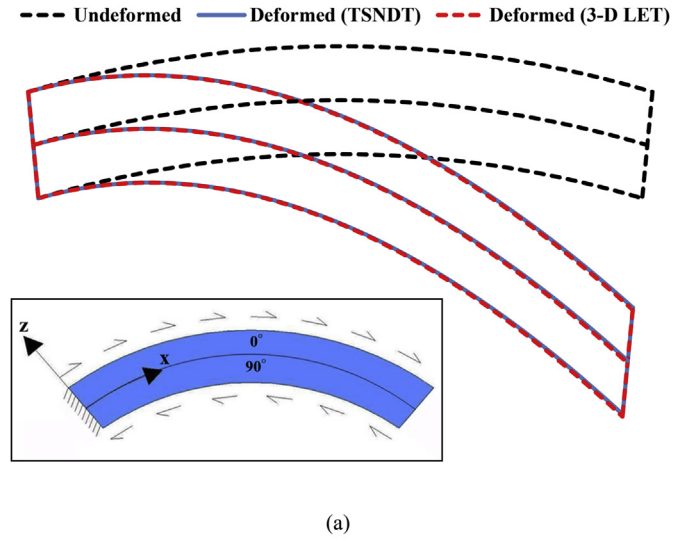


Fig. 4. For a cantilever $90^\circ/0^\circ$ spherical shell subjected to equal and opposite uniform tangential tractions on the two major surfaces, (a) the deformed shape of the cross-section $y = b/2$ with displacements magnified by a factor of 5, and (b) the x- and the z-displacements along the line $y = b/2$ on the shell mid-surface.

but higher than those from the HSDT*. Whereas the HSDT* slightly under-predicts the centroidal deflection, the other three shell theories over-predict it.

3.2. Cross-ply $0^\circ/90^\circ/0^\circ$ laminated spherical shell subjected to sinusoidal distributed normal traction on the top surface

3.2.1. Thin shell

We analyze deformations of a simply supported $0^\circ/90^\circ/0^\circ$ thin and deep laminated spherical shell with $a = b$, $R/a = 1$, $h = 30$ mm and $a/h = 100$, material properties given by Data set 1, and the sinusoidal normal tensile traction given by Eq. (17) applied only on its top surface. We have compared in Fig. 2(a) and (b) the presently computed through-the-thickness distributions of the axial stress, $\sigma_{xx}(0.5a, 0.5b, z)$, the transverse normal stress, $\sigma_{zz}(0.5a, 0.5b, z)$, and the transverse shear stresses $\sigma_{xz}(0, 0.5b, z)$ and $\sigma_{yz}(0.5a, 0, z)$ with those from the analytical solution of Wu and Liu (1994) who employed a LW third order theory. Stresses at points on an edge are found by extrapolation from their values at interior points of the element abutting the edge. The transverse normal stress at the centroid of the shell top

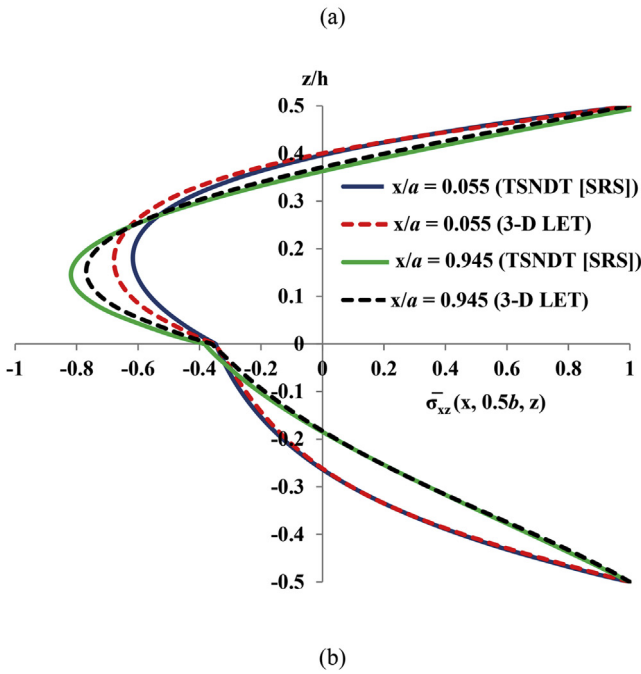
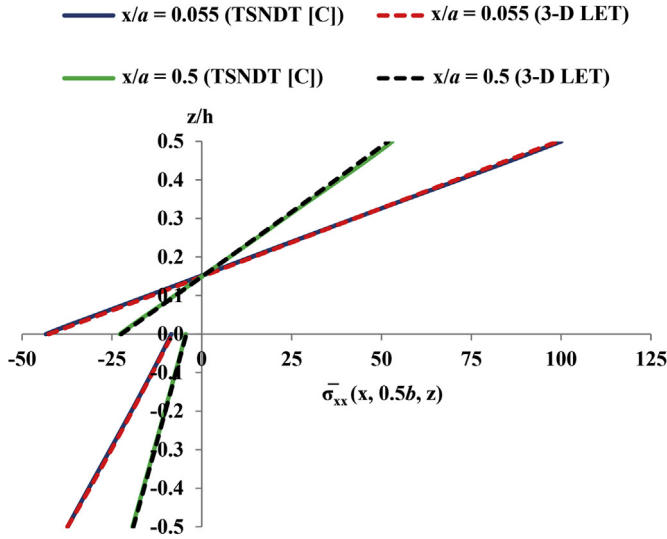


Fig. 5. For a cantilever $90^\circ/0^\circ$ spherical shell subjected to equal and opposite uniform tangential tractions on the two major surfaces, through-the-thickness distributions of (a) $\bar{\sigma}_{xx}(x, 0.5b, z)$ for $x/a = 0.055, 0.5$, and $\bar{\sigma}_{xz}(x, 0.5b, z)$ for $x/a = 0.055$ and 0.945 . Stresses are normalized by q_0 .

surface computed with the TSNDT and the one-step SRS accurately satisfies the normal traction BC with only 0.3% error. Furthermore, for the two solutions, $\|e\|_{\text{sup}}$ equals 1.29%, 3.45% and 2.3% for σ_{xx} , σ_{xz} , and σ_{yz} , respectively. These errors occur at $z/h = 0.5, 0.35$ and 0.43 , respectively, i.e., not at the same point in the shell.

3.2.2. Thick shell

For the shell studied in subsection 3.2.1 but with $a/h = 10$, we have depicted in Fig. 3 through-the-thickness distribution of the transverse shear stress, $\sigma_{yz}(0.5a, 0, z)$, computed from the TSNDT using the one-step SRS, and the analytical solution based on the LW third order theory (Wu and Liu, 1994) and the 3-D LET (Wu et al.,

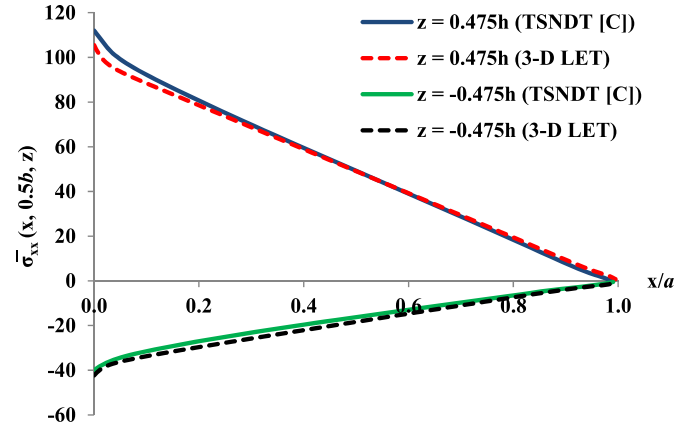


Fig. 6. For a cantilever $90^\circ/0^\circ$ spherical shell subjected to equal and opposite uniform tangential tractions on the two major surfaces, variation of $\bar{\sigma}_{xx}(x, 0.5b, z)$ along the x -direction of the shell for $z/h = \pm 0.475$.

1996). The stress computed using the SRS exactly satisfies the zero traction BCs on the major surfaces. However, the TSNDT and the LW theory predicted σ_{yz} values differ from that of the 3-D LET, respectively, by at most 10.1% and 0.5% at $z = -0.08h$. We note that for a laminate with N layers, the LW theory requires N times the number of independent variables needed for the ESL theory. In order to investigate whether the FE mesh refinement will improve the accuracy of the TSNDT σ_{yz} at the edge, we have included in the Figure results with the uniform FE mesh of 33 elements in the x - and the y - directions and a non-uniform FE mesh of 33 elements in the x - and the y - directions generated using the Chebyshev-Gauss-Lobatto (C-G-L) discretization (Tornabene et al., 2015) with coordinates (x_i, y_j) of a node on the mid-surface given by

$$x_i = \frac{a}{2} \left[1 - \cos\left(\frac{i-1}{I_N-1}\pi\right) \right] \quad (i = 1, 2, \dots, I_N), \quad \text{for } x_i \in [0, a]$$

$$y_j = \frac{b}{2} \left[1 - \cos\left(\frac{j-1}{I_M-1}\pi\right) \right] \quad (j = 1, 2, \dots, I_M), \quad \text{for } y_j \in [0, b]$$

(18)

Here I_N and I_M equal the number of nodes in the x - and the y -directions, respectively. The results from the three FE meshes (including the original uniform FE mesh of 25 elements in the x - and the y - directions) are found to be essentially the same as should be evident from the plots of Fig. 3. We note that when 33 elements are used in the x - and the y -directions of the shell, the length of each element in the uniform mesh is $0.0303a$ whereas that in the non-uniform mesh is $0.0023a$ and $0.0475a$ for the element adjacent to the edge surface and at the center of the shell, respectively. The in-plane normal stress σ_{xx} at the centroids of the top and the bottom surfaces of the shell computed using the non-uniform mesh differs, respectively, by 0.7% and 7.3% from those obtained using the uniform mesh.

3.3. Cross-ply $90^\circ/0^\circ$ laminated spherical shell subjected to equal and opposite uniformly distributed tangential tractions on the two major surfaces

We discern deformations of a $90^\circ/0^\circ$ cross-ply spherical shell with $h = 2$ cm, $a/h = 10$, $a/b = 2$, $R/a = 5$, values of material parameters given by Data set 2, clamped at the edge $x = 0$, the remaining three edges traction free, and subjected to equal and opposite uniform tangential tractions of magnitude $q_0 = 10$ MPa on the two major surfaces as illustrated by the inset in Fig. 4(a). We

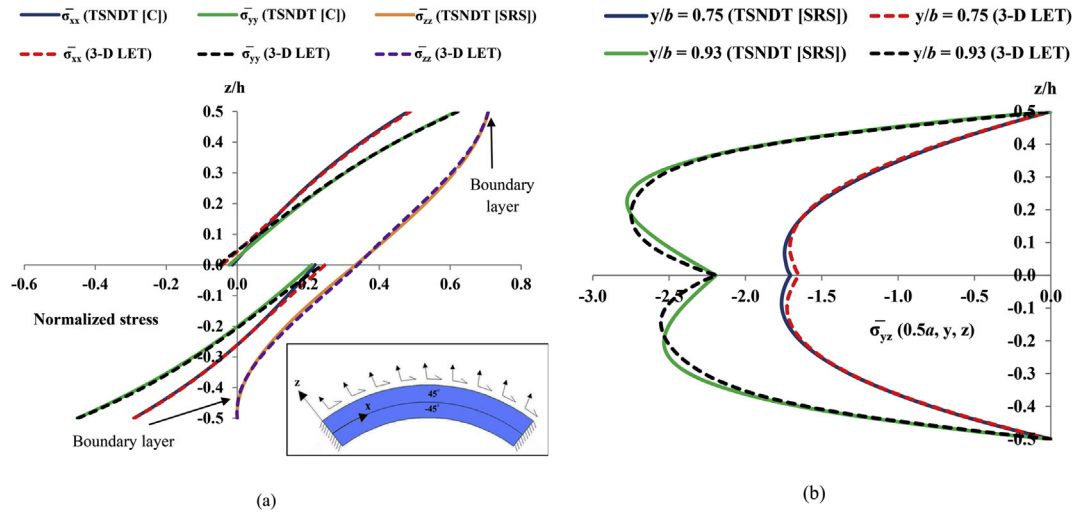


Fig. 7. For a clamped $-45^\circ/45^\circ$ spherical shell subjected to combined normal and tangential uniform tractions on the top surface, through-the-thickness distributions of (a) $\bar{\sigma}_{xx}$, $\bar{\sigma}_{yy}$ and $\bar{\sigma}_{zz}$ at $(0.5a, 0.5b, z)$ and (b) $\bar{\sigma}_{yz}(0.5a, y, z)$ for $y/b = 0.93$ and 0.75 . The transverse stresses are normalized by $q = \sqrt{q_x^2 + q_z^2}$ and the in-plane stresses by $10q$.

have depicted in Fig. 4(a) the deformed shape of the cross-section at $y = b/2$ and in Fig. 4(b) the x - and the z - displacements along the line $y = b/2$ on the shell mid-surface with their scales on the right and the left vertical axes, respectively. The results from the TSNDT are computed using the uniform FE mesh of 45 and 23 elements in the x - and the y - directions, respectively, (38,904 DoF) and those from the 3-D LET with 100, 50 and 5 8-node uniform brick elements per layer in the x -, the y - and the z - directions, respectively, (total 226,644 DoF). The results from the two theories have $\|e\|_{sup} = 1.41\%$ and 1.06% for the x - and the z -displacements, respectively.

In Fig. 5(a) we have displayed through-the-thickness distributions of the axial stress, σ_{xx} , along transverse normal sections near and away from the clamped edge. The axial stress computed from the TSNDT and the 3-D LET agree well with each other having the

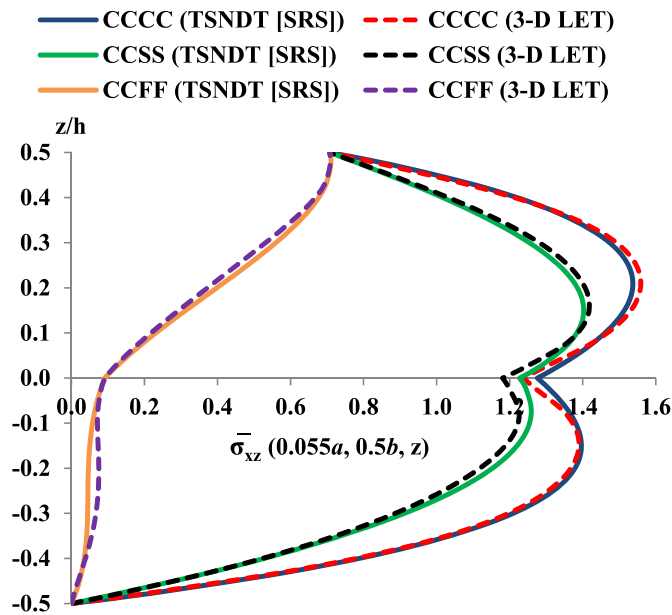


Fig. 8. For a $-45^\circ/45^\circ$ spherical shell subjected to combined uniform normal and tangential tractions on the top surface, through-the-thickness distribution of $\bar{\sigma}_{xx}(0.055a, 0.5b, z)$ for three different BCs. The stresses are normalized by $q = \sqrt{q_x^2 + q_z^2}$.

maximum difference, $\|e\|_{sup}$, of 4% and 3.65% along points $(0.055a, 0.5b, z)$ and $(0.5a, 0.5b, z)$, respectively; these differences occur at $z/h = 0^+$. The magnitude of the axial stress on the top surface at $x = 0.055a$ is about twice that at $x = 0.5a$. In Fig. 5(b) we have portrayed through-the-thickness distributions of the TSNDT transverse shear stress, σ_{xz} , computed using the SRS along the transverse normal in the plane $y = b/2$ located at $0.055a$ from the edges $x = 0$ and $x = a$ and those obtained by analyzing 3-D deformations of the shell. The two sets of results differ at most by 7.2% and 9.9% along the sections $x = 0.055a$ and $x = 0.945a$, respectively. The transverse shear stress computed on the top surface differs from the applied tangential traction by at most 5.74% at $x = 0.945a$ near the traction free edge. However, near the clamped edge, $x = 0.055a$, this error is only 0.67%.

In Fig. 6 we have depicted the variation of σ_{xx} in the plane $y = b/2$ along the x - direction of the shell at $z = \pm 0.475 h$. The results from the TSNDT and the 3-D LET are in good agreement with each other differing at most by 6.2% and 5.6% at $z = \pm 0.5 h$ on the clamped edge. At the free edge, $x = a$, σ_{xx} accurately satisfies the zero normal traction BC. The axial stress is maximum at the clamped edge, first rapidly and then linearly decreases with an increase in the distance from the clamped edge. Results not included herein suggest that the shell curvature strongly influences magnitudes of the axial stress induced at the clamped edge in the top and the bottom layers.

3.4. Angle-ply $-45^\circ/45^\circ$ laminated spherical shell subjected to combined uniform normal and tangential tractions on the top surface

We analyze deformations of an angle-ply $-45^\circ/45^\circ$ laminated spherical shell of the same geometry and material as those considered in subsection 3.3 but with all edges clamped and loaded only on the top surface with uniform normal (q_z) and tangential (q_x) tractions, each of magnitude 10 MPa. Using the same FE meshes as those for the problem studied in subsection 3.3, we have displayed in Fig. 7(a) through-the-thickness distributions of the normal stresses (σ_{xx} , σ_{yy} , σ_{zz}) along the transverse normal passing through the centroid of the mid-surface; the inset depicts the schematic of the problem studied. The results from the TSNDT and the LET agree well with each other and the average difference norm, $\|e\|_0$, equals 5.2%, 4.5% and 1.6% for σ_{xx} ,

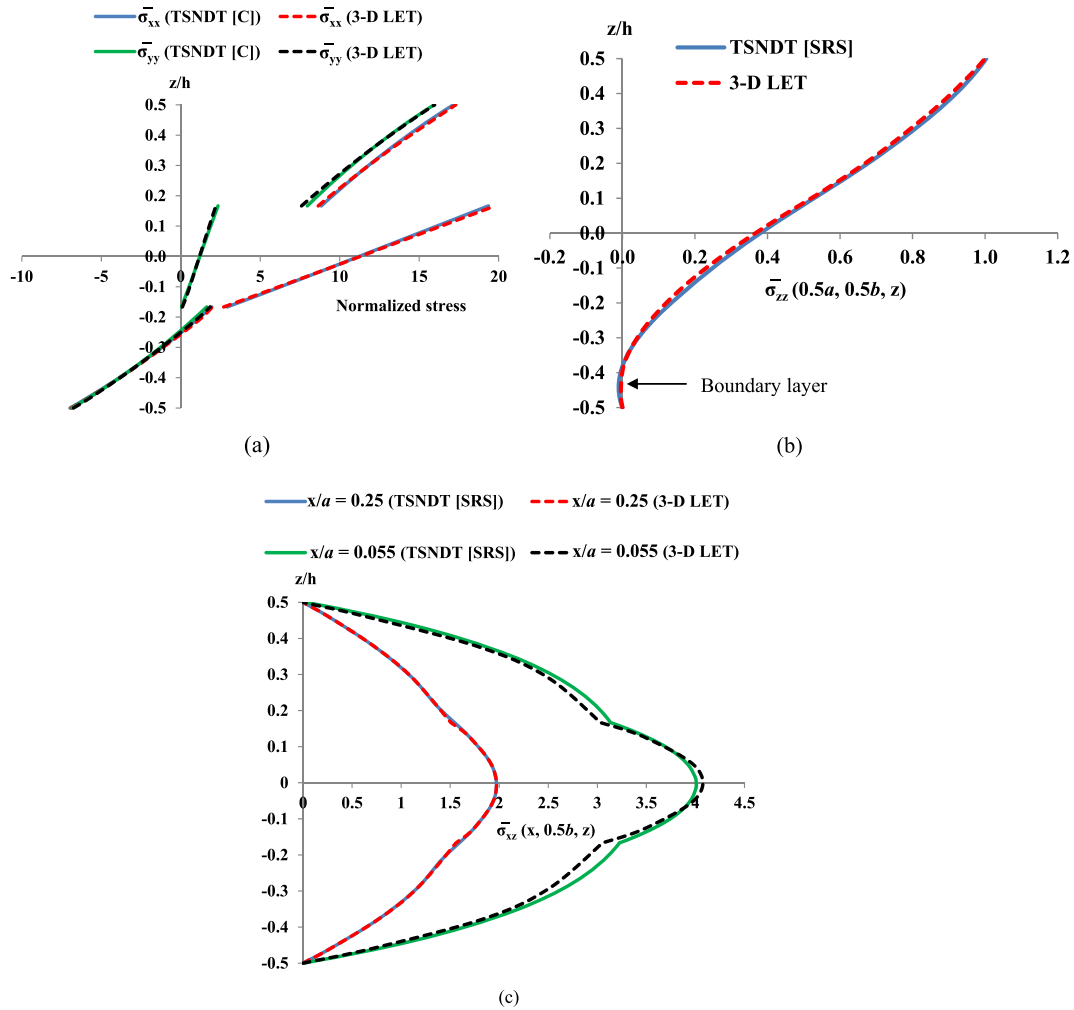


Fig. 9. For a clamped $45^\circ/0^\circ/45^\circ$ doubly curved shell subjected to a uniform normal tensile traction q_0 on its top surface, through-the-thickness distributions of (a) $\bar{\sigma}_{xx}(0.5a, 0.5b, z)$ and $\bar{\sigma}_{yy}(0.5a, 0.5b, z)$, (b) $\bar{\sigma}_{zz}(0.5a, 0.5b, z)$, and (c) $\bar{\sigma}_{xz}(0.055a, 0.5b, z)$ and $(0.25a, 0.5b, z)$. Stresses are normalized by q_0 .

$\bar{\sigma}_{yy}$ and $\bar{\sigma}_{zz}$, respectively. It can be seen that the transverse normal stress computed using the SRS accurately captures the “boundary

layer” phenomenon near major surfaces of the shell as predicted by the 3-D LET and the prescribed normal traction BC is accurately satisfied on the top surface of the shell with only 0.11% error at the centroid. In Fig. 7(b) we have depicted through-the-thickness distributions of the transverse shear stress, σ_{yz} , near and away from the edge $y = b$ along the transverse normal passing through points $(0.5a, 0.93b, 0)$ and $(0.5a, 0.75b, 0)$. It is found that near the edge at $y = 0.93b$, the maximum and the average differences between results from the two theories are 4.42% and 2.75%, respectively. These differences diminish to 3.32% and 2.05% at $y = 0.75b$. We note that the maximum differences between the two sets of results occur at $z/h = -0.075$ and 0 for $y/b = 0.93$ and 0.75 , respectively. The maximum value, $2.8q$, of σ_{yz} at $y/b = 0.93$, $z/h = 0.225$ is significantly more than the maximum value, $1.7q$, at $y/b = 0.75$, $z/h = \pm 0.075$, where q is the magnitude of the applied surface traction. Whereas the distribution of σ_{yz} about $z = 0$ is symmetric on the plane $y/b = 0.75$, it is asymmetric on the plane $y/b = 0.93$.

Shells with CCSS and CCFF edges. In Fig. 8 we have depicted through-the-thickness distribution of the transverse shear stress, σ_{xz} , along the transverse normal passing through the point $(0.055a, 0.5b, 0)$ near the edge $x = 0$ for the shell with edges $y = 0$ and b clamped (C) and edges $x = 0$ and a either simply supported (S) or traction free (F); the corresponding results are denoted by labels

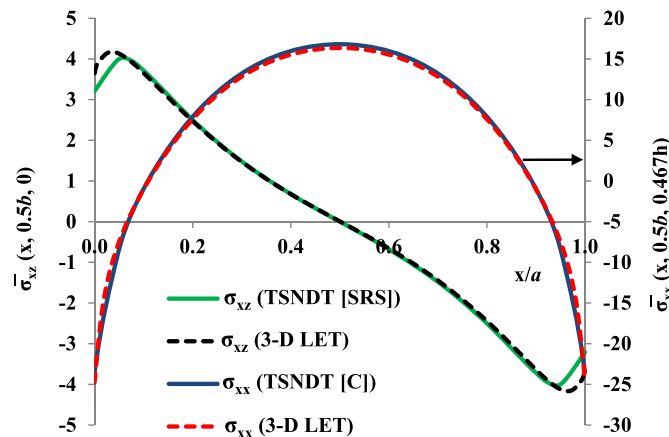


Fig. 10. For a clamped $45^\circ/0^\circ/45^\circ$ doubly curved shell subjected to a uniform normal tensile traction on its top surface, variation of $\bar{\sigma}_{xz}(x, 0.5b, 0.467h)$ and $\bar{\sigma}_{xx}(x, 0.5b, 0)$ along the length in the x -direction of the shell. Stresses are normalized by q_0 .

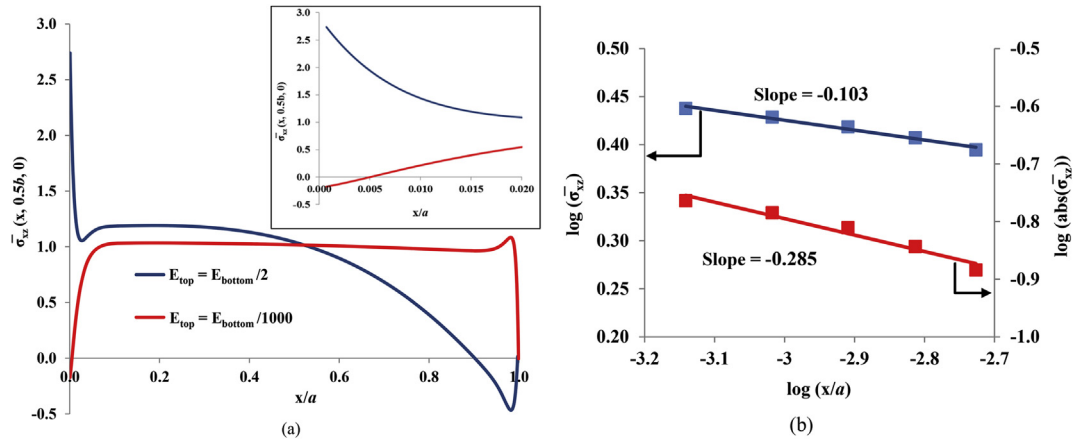


Fig. 11. For a cantilever curved beam ($a/h = 5$) made of two layers of dissimilar isotropic materials and subjected to equal and opposite uniform tangential tractions q_0 on the two major surfaces, (a) variation of $\bar{\sigma}_{xz}(x, 0.5b, 0)$ along the length in the x -direction of the shell, and (b) on the log-log scale $\bar{\sigma}_{xz}(x, 0.5b, 0)$ vs. the normalized distance, x/a , from the edge $x = 0$. The stress is normalized by q_0 .

CCSS and CCFF in the Figure. The norm, $\|e\|_0$, for results computed from the TSNDT SRS and the 3-D LET equals 1.58%, 2.45% and 4.74% for the CCCC, the CCSS and the CCFF shells, respectively. The transverse shear stress computed using the SRS accurately satisfies the tangential traction BC on the top surface of the shell having less than 0.05% error at the point $(0.055a, 0.5b, 0.5h)$ for the three BCs. This indicates that, as for laminated plates analyzed by Vel and Batra (1999) using the Eshelby-Stroh formalism, the stress distribution near an edge depends on the BC specified on that edge. For the three BCs studied, the maximum value of the transverse shear stress at a point near the edge $x = 0$ is the largest for the clamped BC and the smallest for the traction free BC specified on that edge. For each set of BCs the variation of σ_{xz} versus z is asymmetric about $z = 0$.

3.5. Angle-ply $45^\circ/0^\circ/45^\circ$ laminated doubly curved shell subjected to uniform normal traction on the top surface

We now study deformations of a clamped angle-ply $45^\circ/0^\circ/45^\circ$ shell with $h = 3$ cm, $a = b$, $a/h = 10$, $R_{1m} = 2a$, $R_{2m} = 2R_{1m}$, values of material parameters listed in Data set 2, and subjected to a uniform normal tensile traction, $q_0 = 10$ MPa, only on its top surface. As mentioned in the Introduction, R_{1m} and R_{2m} are the principal radii of curvature of the mid-surface of the shell. This shell geometry is obtained by first drawing two curves of radii $R_{1t} = R_{1m} + h/2$ and $R_{1b} = R_{1m} - h/2$ with the included angle $= a/R_{1m}$. Taking these two curves as segments of two concentric circles, we revolve them about the horizontal axis in the plane of the concentric circles and passing through their centre by the

angle $= b/R_{2m}$. In Fig. 9(a) and (b) we have exhibited through-the-thickness distributions of the in-plane normal stresses and the transverse normal stress, respectively, along the transverse normal passing through the centroid of the mid-surface. The TSNDT stress σ_{xx} (σ_{yy}) differs from the 3-D LET stress by at most 8.14% (4.78%); this maximum difference occurs at the interface between the middle and the bottom (top) layers. The transverse normal stress computed using the SRS differs from the prescribed normal traction at the centroid of the top surface by only 0.31% and exhibits boundary layers near the two major surfaces. We note that the 3-D FE results are obtained with 100, 100 and 5 uniform 8-node brick elements for each layer in the x -, the y - and the z - directions, respectively (total 550,854 DoF). In Fig. 9(c) we have exhibited through-the-thickness distribution of the TSNDT and the LET transverse shear stress, σ_{xz} , along the transverse normal passing through points $(0.055a, 0.5b, 0)$ and $(0.25a, 0.5b, 0)$. The two sets of results qualitatively agree very well, and quantitatively differ from each other at most by 5.33% (3.46%) for $x = 0.055a$ ($x = 0.25a$); this maximum difference occurs at the interface between the middle and the bottom (top) layers.

In Fig. 10 we have exhibited variations of σ_{xz} and σ_{xx} along the line parallel to the x - axis in the plane $y = b/2$ located at $z = 0$ and $0.467h$, respectively, with their scales shown on the left and the right vertical axis. The TSNDT captures the boundary layer effect in σ_{xz} as predicted by the 3-D LET near the clamped edges. However, σ_{xz} (σ_{xx}) obtained by the SRS (the TSNDT constitutive relation) at the edge $x = 0$ differs from that of the LET by 12.1% (3.1%) and at $x/a = 0.1$ by 2.9% (2.5%). Near the clamped edge the magnitude of σ_{xz} equals about 16% of σ_{xx} .

Table 5
The relative change in the stress $\sigma_{xz}(x = x_0)/\sigma_{xz}(x)$ as the distance from the clamped edge, x , is decreased to $x_0 = 0.000722a$ in the singular region with $\lambda = 0.106$.

x/a	x_0/x	Analytical (Ma and Wu, 1990)	TSNDT	%Diff.	Is point in singularity dominated region?
0.020100	0.036	1.4227	2.5171	-76.92	No
0.010172	0.071	1.3236	1.9192	-44.99	No
0.007130	0.101	1.2747	1.6238	-27.38	No
0.005201	0.139	1.2328	1.4283	-15.86	No
0.003574	0.202	1.1847	1.2660	-6.86	Yes
0.002658	0.272	1.1481	1.1773	-2.55	Yes
0.002250	0.321	1.1280	1.1388	-0.95	Yes
0.001877	0.385	1.1065	1.1040	0.23	Yes
0.001537	0.470	1.0834	1.0728	0.97	Yes
0.001232	0.586	1.0582	1.0452	1.23	Yes
0.000960	0.752	1.0306	1.0209	0.94	Yes

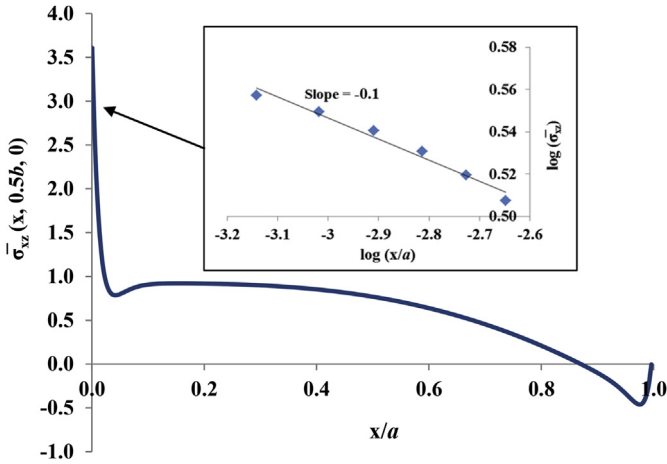


Fig. 12. For a cantilever curved beam ($a/h = 7$) made of two layers of dissimilar isotropic materials and subjected to equal and opposite uniform tangential tractions q_0 on the two major surfaces, variation of $\bar{\sigma}_{xz}(x, 0.5b, 0)$ along the length in the x -direction of the shell. The stress is normalized by q_0 .

3.6. Stress singularity in laminated shells of dissimilar isotropic materials

In a laminate stresses may be singular at points where the major surfaces and the layer interfaces intersect the laminate edges. For a laminated shell made of layers of dissimilar materials the order of this stress singularity at the apex of the layer interface depends on the material parameters. Williams (1952) predicted that stresses near the apex of an isotropic elastic wedge are proportional to $r^{-\lambda}$, where r is the distance from the apex and λ is the order of the singularity which depends upon the material parameters and the wedge angle. For the plane stress/strain deformations of wedges made of two dissimilar isotropic, homogeneous and linear elastic materials and perfectly bonded together along a common edge, Bogy (1971) as well as Ma and Wu (1990) have provided expressions to compute λ at the intersection of the layer interface and the wedge surface with the traction and the displacement BCs, respectively.

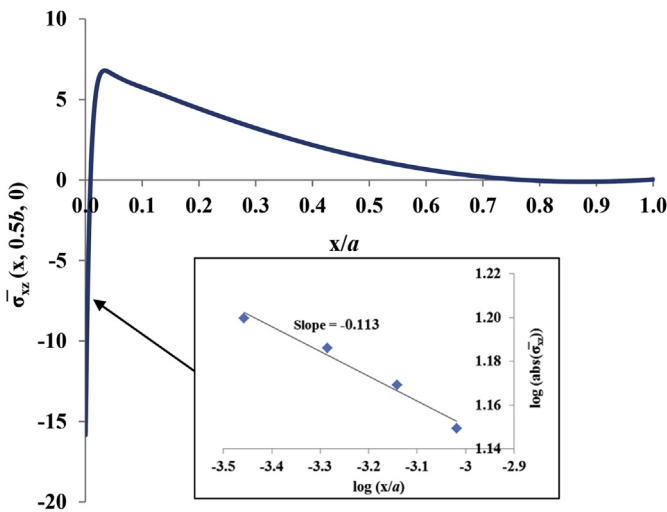


Fig. 13. For a cantilever curved beam ($a/h = 5$) made of two layers of dissimilar isotropic materials and subjected to uniform normal tensile traction q_0 on the top surface, variation of $\bar{\sigma}_{xz}(x, 0.5b, 0)$ along the length in the x -direction of the shell. The stress is normalized by q_0 .

We consider a shell comprised of two layers of dissimilar isotropic materials and study plane strain deformations by constraining the y -displacement of all shell particles to zero. The elastic constants of the bottom layer material $(E_{\text{bottom}}, \nu_{\text{bottom}}) = (210 \text{ GPa}, 0.3)$ and those of the top layer material $(E_{\text{top}}, \nu_{\text{top}}) = (E_{\text{bottom}}/2, 0.3)$ for case 1 and equal to $(E_{\text{bottom}}/1000, 0.3)$ for case 2. The analytical values of the order λ of stress singularity near the clamped edge, $x = 0$, given in Ma and Wu (1990) are 0.106 and 0.288 for cases 1 and 2, respectively.

We have computed the value of λ using the TSNDT coupled with the SRS for two example problems: (i) equal and opposite uniform tangential tractions specified on the two major surfaces of the shell with $R/a = 5$, $h = 20 \text{ mm}$, $a/h = 10$ and 7 and (ii) uniform normal tensile traction applied only on the top surface of the shell with $R/a = 5$, $h = 20 \text{ mm}$ and $a/h = 5$. Since the value of λ does not depend upon geometric variables of the shell and loading conditions on the major surfaces, λ computed for the two problems should be the same. However, the magnitude of the stress intensity factor at the edge may depend upon these parameters as pointed out by Qian and Akisanya (1999). We have not computed the stress intensity factor.

3.6.1. Equal and opposite uniform tangential tractions, q_0 , on the two major surfaces

In Fig. 11(a) we have exhibited for the shell with $a/h = 5$ and for the two sets of material properties the variation of σ_{xz} with the distance from the point on the clamped edge that is on the interface between the two adjoining layers; the inset shows the region between $x = 0$ and $0.02a$. We have used the C-G-L grid with 381 elements to obtain a very fine mesh near the shell edges. The nearest point from the edge at which the TSNDT stress is computed has $x_0 = 7.22\text{E-}04a$. From results plotted in the Figure one concludes that the singularity dominant region is bounded by $x/a < 0.02$ in which the stress also exhibits a boundary layer effect. The analytical solution, $\lambda = 0.106$, for case 1 of material properties implies that the shear stress at two points should satisfy $\sigma_{xz}(x = x_1)/\sigma_{xz}(x = x_2) = (x_1/x_2)^{-0.106} = p$. In Table 5 we have compared at different points values of p found from the analytical and the TSNDT solutions. These results suggest that if the point is moved from $x = 0.0102a$ to $7.22\text{E-}04a$, i.e., the distance is decreased by a factor of ≈ 14 , the stress should increase by 32.4%. However, the numerical solution predicts the increase in the stress to be 92%. Thus, the point located at a distance from the clamped edge as close as 1% of the edge length is not affected by the singularity. We note that in the singularity region near a crack tip (i.e., $\lambda = 0.5$), if the distance between two points is decreased by a factor of 14, the stress will increase by 274% as compared to 32% in the present problem. As the point is moved further close to the edge $x = 0$, we see from Table 5 that in the region $x/a < 0.0036$ the relative change in the stress predicted from the analytical and the TSNDT solutions agree well with less than 7% difference. Thus one may conclude that the singularity dominates in a very small region ($x/a < 0.0036$) near the clamped edge. By a similar argument we find for the set 2 of material properties that the singularity affected region is $x/a < 0.0023$.

In Fig. 11(b) we have depicted on a log-log scale the variation of the normalized stress, $\bar{\sigma}_{xz} = \sigma_{xz}/q_0$, with the normalized distance, x/a , from the clamped edge for cases 1 and 2 with their scales shown on the left and the right vertical axes, respectively. Since $\bar{\sigma}_{xz}$ has negative sign near the edge for case 2 of material parameters, the logarithm of its absolute value is computed. A line is fitted through $(\log(\text{abs}(\bar{\sigma}_{xz})), \log(x/a))$ data points using the least squares method and the regression coefficient is found to be 0.98 and 0.96 for cases 1 and 2, respectively. The magnitude of the slope of this

line equals the order of singularity, λ , which is found to be 0.103 and 0.285 for cases 1 and 2 differing from their analytical solutions by 2.83% and 1.04%, respectively. We note that Qian and Akisanya (1999) and Chadegani and Batra (2011), amongst others, have used this approach to compute the order of stress singularity with the FEM near an edge. Near the traction free edge, $x = a$, the boundary layer phenomenon is observed, however, σ_{xz} is not singular in this boundary layer region since it is identically zero on the edge.

In order to demonstrate that the order of stress singularity does not depend upon the geometric parameters, we have depicted in Fig. 12 for a thinner shell with $a/h = 7$ the variation of σ_{xz} along the layer interface for the set 1 of material properties. The inset in the Figure shows results in the vicinity of the clamped edge, $x = 0$, on a log-log scale and the regression coefficient of the line fitted using the least squares method through $(\log(\bar{\sigma}_{xz}), \log(x/a))$ data points is 0.97. The order 0.1 of singularity differs from the analytical value of 0.106 by ~6%.

3.6.2. Uniform normal tensile traction on the top surface

In order to demonstrate that the order of stress singularity does not depend upon the loading conditions on the major surfaces, we now study deformations of a shell with $a/h = 10$ and subjected to a uniform normal tensile traction, q_0 , only on the top surface. In Fig. 13 we have portrayed the variation of σ_{xz} at the interface with the distance from the clamped edge, $x = 0$, for the set 1 of material properties; the inset shows a plot of $\log(\bar{\sigma}_{xz})$ versus $\log(x/a)$ in a neighborhood of the edge with the least squares line having the regression coefficient of 0.97 fitted through data points. The computed order 0.113 of singularity differs from the analytical value 0.106 by 6.6%.

4. Conclusions

Static infinitesimal deformations of doubly curved, laminated, linearly elastic and orthotropic shells have been analyzed by using a third order shear and normal deformable shell theory (TSNDT) and the finite element method (FEM). The in-plane stresses are computed from constitutive relations and the shell theory displacements. The transverse shear and the transverse normal stresses are computed with a one-step stress recovery scheme (SRS). It is found that stresses computed from the TSNDT at interior points (situated at a distance greater than 1% of the span from an edge) differ by less than 5% from those found by analyzing the 3-D deformations of the shell. The transverse normal stress computed from the SRS exhibits the boundary layer effect near the major surfaces of the shell and satisfies well the normal traction boundary condition (BC) on the major surfaces with less than 0.5% error. For simply supported symmetric and anti-symmetric cross-ply shells, the deflections predicted by the TSNDT differ from the corresponding 3-D linear elasticity theory (LET) solutions by about 9% (3%) for the span to thickness ratio (a/h) = 5 (10) and the radius of curvature to span ratio (R/a) = 2. For a three layer symmetric cross-ply shell with $R/a = 1$ the deflections computed from the two theories differ at most by 4% for a/h between 5 and 100. For a four layer symmetric cross-ply shell with $a/h = 10$ the deflections predicted by the TSNDT and the 3-D LET differ by about 7% for $R/a = 1$ and this difference decreases with an increase in the shell curvature.

For a three layer symmetric cross-ply simply supported shell with $R/a = 1$ and $a/h = 10$, transverse shear stress, σ_{yz} , at the edge $y = 0$ computed using the SRS differs from that predicted by the 3-D LET by ~10%. However, this difference reduces to ~2% for a thin shell with $a/h = 100$. For a two layer anti-symmetric cross-ply cantilever

shell subjected to equal and opposite tangential tractions on the top and the bottom surfaces, the axial stress, σ_{xx} , at the clamped edge obtained from the two theories differs by ~6%. The transverse shear stress computed using the SRS in the vicinity of the traction free (clamped) edge differs from the 3-D LET value at most by 10% (7%) and it differs from the applied tangential traction by ~6% (0.7%).

For a two layer anti-symmetric angle-ply shell with edges $y = 0$ and b simply-supported and subjected to a combined normal and tangential tractions, the TSNDT transverse shear stress, σ_{xz} , differs, respectively, from the 3-D LET solution by ~1.6%, 2.5% and 4.7% near the edge $x = 0$ for clamped, simply supported and traction free edge $x = 0$. For a three layer angle-ply clamped shell, the transverse shear stress at an edge differs by ~12% from the corresponding 3-D LET solution and this difference decreases to 3% at $x = 0.1a$.

For a cantilever curved beam made of two layers of dissimilar isotropic materials, the order of singularity in the stress near the clamped edge computed from the TSNDT and the SRS differs from the corresponding analytical solution by less than 7% for the ratio of Young's moduli of the two materials equalling 2 and 1000. The singularity is dominant in a very small region (~0.36% of the edge length) near the edge.

Acknowledgements

Authors are grateful to the two anonymous reviewers and the editor for their constructive comments on the earlier version of the manuscript that have helped improve upon the presentation of the work. This work was partially supported by the US Office of Naval Research (ONR) grant N00014-16-1-2309 with Dr. Y.D.S. Rajapakse as the Program Manager. Views expressed in the paper are those of the authors and neither of the ONR nor of Virginia Tech.

References

- Ambartsumian, S.A., 1962. Contributions to the theory of anisotropic layered shells. *Appl. Mech. Rev.* 15 (4), 245–249.
- Ambartsumian, S.A., 2002. Nontraditional theories of shells and plates. *Appl. Mech. Rev.* 55 (5), 35–44.
- Antman, S.S., 1972. The theory of rods. In: Truesdell, C. (Ed.), *Handbuch der Physik*, vol. VI a/2. Springer, Berlin.
- Bathe, K.J., 1996. *Finite Element Procedures*. Pearson Education, Inc. Publishing.
- Batra, R.C., Aimmancee, S., 2005. Vibrations of thick isotropic plates with higher order shear and normal deformable plate theories. *Comput. Struct.* 83, 934–955.
- Batra, R.C., Vidoli, S., 2002. Higher-order piezoelectric plate theory derived from a three-dimensional variational principle. *AIAA J.* 40 (1), 91–104.
- Batra, R.C., Xiao, J., 2013. Analysis of post-buckling and delamination in laminated composite St. Venant-Kirchhoff beams using CZM and layerwise TSNDT. *Compos. Struct.* 105, 369–384.
- Batra, R.C., Vidoli, S., Vestroni, F., 2002. Plane waves and modal analysis in higher-order shear and normal deformable plate theories. *J. Sound Vib.* 257 (1), 63–88.
- Bert, C.W., 1980. Analysis of shells, analysis and performance of composites. In: Broutman, L.J. (Ed.), Wiley, New York, N.Y., pp. 207–258.
- Bogy, D.B., 1968. ge-bonded dissimilar orthogonal elastic wedges under normal and shear loading. *J. Appl. Mech.* 35 (3), 460–466.
- Bogy, D.B., 1971. Two edge-bonded elastic wedges of different materials and wedge angles under surface tractions. *J. Appl. Mech.* 38 (2), 377–386.
- Carrera, E., 2003. Historical review of Zig-Zag theories for multilayered plates and shells. *Appl. Mech. Rev.* 56 (3), 287–308.
- Carrera, E., Cinefra, M., Petrolo, M., Zappino, E., 2014. Finite Element Analysis of Structures through Unified Formulation. John Wiley & Sons.
- Chadegani, A., Batra, R.C., 2011. Analysis of adhesive-bonded single-lap joint with an interfacial crack and a void. *Int. J. Adhes. Adhes.* 31 (6), 455–465.
- Chaudhuri, R.A., Seide, P., 1987. An approximate semi-analytical method for prediction of interlaminar shear stresses in an arbitrarily laminated thick plate. *Comput. Struct.* 25 (4), 627–636.
- Donnell, L.H., 1933. Stability of thin-walled tubes under torsion. *NACA Rep.* 479.
- Dundurs, J., 1969. Discussion: "Edge-bonded dissimilar orthogonal elastic wedges under normal and shear loading" (Bogy, DB, 1968, ASME J. Appl. Mech., 35, pp. 460–466). *J. Appl. Mech.* 36 (3), 650–652.
- Fan, J., Zhang, J., 1992. Analytical solutions for thick, doubly curved, laminated shells. *J. Eng. Mech.* 118 (7), 1338–1356.
- Flügge, W., 1973. *Stresses in Shells*, second ed. Springer, NY.
- Huang, N.N., 1994. Influence of shear correction factors in the higher order shear

- deformation laminated shell theory. *Int. J. Solids Struct.* 31 (9), 1263–1277.
- Kant, T., Swaminathan, K., 2000. Estimation of transverse/interlaminar stresses in laminated composites—a selective review and survey of current developments. *Compos. Struct.* 49, 65–75.
- Kapania, R.K., 1989. Review on the analysis of laminated shells. *J. Press. Vessel Technol.* 111, 88–96.
- Koiter, W.T., 1960. A consistent first approximation in the general theory of thin elastic shells. *Theory Thin Elastic Shells* 12–33.
- Leissa, A.W., 1973. *Vibration of Shells*, NASA SP-288. US Government Printing Office, Washington DC. Reprinted by the Acoust Soc of Am, 1993.
- Liew, K.M., Lim, C.W., 1996. A higher-order theory for vibration of doubly curved shallow shells. *ASME, J. Appl. Mech.* 63, 587–593.
- Liew, K.M., Lim, C.W., Kitipornchai, S., 1997. Vibration of shallow shells: a review with bibliography. *Appl. Mech. Rev.* 50 (8), 431–444.
- Lo, K.H., Christensen, R.M., Wu, E.M., 1977. A high-order theory of plate deformation—part 2: laminated plates. *J. Appl. Mech.* 44 (4), 669–676.
- Lo, K.H., Christensen, R.M., Wu, E.M., 1978. Stress solution determination for high order plate theory. *Int. J. Solids Struct.* 14, 655–662.
- Love, A.E.H., 1888. Small free vibrations and deformations of thin elastic shells. *Phil. Trans. R. Soc. Ser. A* 179, 491–549.
- Ma, C.C., Wu, H.W., 1990. Analysis of inplane composite wedges under traction-displacement or displacement-displacement boundary conditions. *Acta Mech.* 85 (3–4), 149–167.
- Mindlin, R.D., 1951. Influence of rotatory inertia and shear in flexural motions of isotropic elastic plates. *ASME J. Appl. Mech.* 18, 1031–1036.
- Mindlin, R.D., Medick, M.A., 1959. Extensional vibrations of elastic plates. *J. Appl. Mech.* 26 (4), 561–569.
- Murty, A.K., 1977. Higher order theory for vibrations of thick plates. *AIAA J.* 15 (12), 1823–1824.
- Naghdi, P.M., 1973. *The Theory of Shells and Plates*. Springer, Berlin Heidelberg, pp. 425–640.
- Noor, A.K., Burton, W.S., Peters, J.M., 1990. Predictor–corrector procedures for stress and free vibration analyses of multilayered composite plates and shells. *Comput. Methods Appl. Mech. Eng.* 82, 341–363.
- Noor, A.K., Burton, W.S., Peters, J.M., 1991. Assessment of computational models for multilayered composite cylinders. *Int. J. Solids Struct.* 27 (10), 1269–1286.
- Pagano, N.J., 1970. Exact solutions for rectangular bidirectional composites and sandwich plates. *J. Compos. Mater.* 4 (1), 20–34.
- Pryor, C.W., Barker, R.M., 1971. A finite element analysis including transverse shear effects for application to laminated plates. *AIAA-J.* 9 (5), 912–917.
- Qatu, M.S., 2004. *Vibration of Laminated Shells and Plates*. Elsevier, Amsterdam.
- Qatu, M.S., Asadi, E., Wang, W., 2012. Review of recent literature on static analyses of composite shells: 2000–2010. *Open J. Compos. Mater.* 2 (3), 61–86.
- Qian, Z.Q., Akisanya, A.R., 1999. Wedge corner stress behaviour of bonded dissimilar materials. *Theor. Appl. Fract. Mech.* 32 (3), 209–222.
- Qian, L.F., Batra, R.C., 2004. Transient thermoelastic deformations of a thick functionally graded plate. *J. Therm. Stress.* 27, 705–740.
- Qian, L.F., Batra, R.C., Chen, L.M., 2003. Free and forced vibrations of thick rectangular plates by using higher-order shear and normal deformable plate theory and meshless petrov-galerkin (MLPG) method. *Comput. Model. Eng. Sci.* 4, 519–534.
- Reddy, J.N., 1984. Exact solutions of moderately thick laminated shells. *J. Eng. Mech.* 110 (5), 794–809.
- Reddy, J.N., 1993. An evaluation of equivalent-single-layer and layerwise theories of composite laminates. *Compos. Struct.* 25 (1–4), 21–35.
- Reddy, J.N., Arciniega, R.A., 2004. Shear deformation plate and shell theories: from Stavsky to present. *Mech. Adv. Mater. Struct.* 11 (6), 535–582.
- Reddy, J.N., Liu, C.F., 1985. A higher-order shear deformation theory of laminated elastic shells. *Int. J. Eng. Sci.* 23 (3), 319–330.
- Reissner, E., 1947. Small Bending and Stretching of Sandwich Type Shells. National Advisory Committee for Aeronautics Technical Note No. 1832.
- Rohwer, K., Friedrichs, S., Wehmeyer, C., 2005. Analyzing laminated structures from fibre-reinforced composite material – an assessment. *Tech. Mech.* 25 (1), 59–79.
- Saada, A.S., 2009. *Elasticity: Theory and Applications*. J. Ross Publishing.
- Sanders Jr., J.L., 1959. An Improved First-approximation Theory for Thin Shells. NASA Technical Report R-24.
- Shah, P.H., Batra, R.C., 2015. Through-the-thickness stress distributions near edges of composite laminates using stress recovery scheme and third order shear and normal deformable theory. *Compos. Struct.* 131, 397–413.
- Tornabene, F., Fantuzzi, N., Viola, E., Batra, R.C., 2015. Stress and strain recovery for functionally graded free-form and doubly-curved sandwich shells using higher-order equivalent single layer theory. *Compos. Struct.* 119, 67–89.
- Vel, S.S., Batra, R.C., 1999. Analytical solution for rectangular thick laminated plates subjected to arbitrary boundary conditions. *AIAA J.* 37 (11), 1464–1473.
- Vel, S.S., Batra, R.C., 2002. Exact solutions for thermoelastic deformations of functionally graded thick rectangular plates. *AIAA J.* 40, 1421–1433.
- Vidoli, S., Batra, R.C., 2000. Derivation of plate and rod equations for a piezoelectric body from a mixed three-dimensional variational principle. *J. Elast.* 59 (1–3), 23–50.
- Wang, X., Li, S.J., 1992. Analytic solution for interlaminar stresses in a multi-laminated cylindrical shell under thermal and mechanical loads. *Int. J. Solids Struct.* 29 (10), 1293–1302.
- Williams, M.L., 1952. Stress singularities resulting from various boundary conditions. *J. Appl. Mech.* 19 (4), 526–528.
- Wu, C.P., Kuo, H.C., 1992. Interlaminar stress analysis for laminated composite plates based on a local higher-order lamination theory. *Compos. Struct.* 20 (4), 237–247.
- Wu, C.P., Liu, C.C., 1994. Stress and displacement of thick doubly curved laminated shells. *J. Eng. Mech.* 120 (7), 1403–1428.
- Wu, C.P., Tarn, J.Q., Chi, S.M., 1996. Three-dimensional analysis of doubly curved laminated shells. *J. Eng. Mech.* 122 (5), 391–401.
- Xiao, J., Batra, R.C., 2014. Delamination in sandwich panels due to local water slamming loads. *J. Fluids Struct.* 48, 122–155.
- Xiao-ping, S., 1996. An improved simple higher-order theory for laminated composite shells. *Comput. Struct.* 60 (3), 343–350.